NASA CR-54544
PWA FR-1713

SINGLE STAGE EXPERIMENTAL EVALUATION OF SLOTTED ROTOR AND STATOR BLADING

PART I - ANALYSIS AND DESIGN

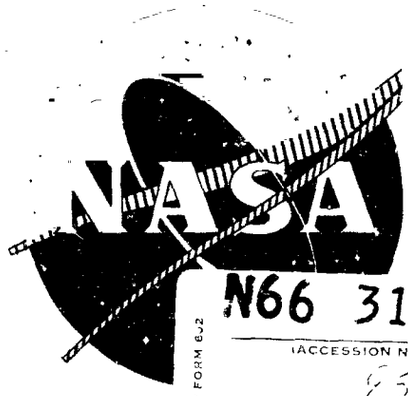

PREPARED FOR
NATIONAL AERONAUTICS AND SPACE ADMINISTRATION
CONTRACT NAS3-7603

Pratt & Whitney Aircraft DIVISION OF UNITED AIRCRAFT CORPORATION
FLORIDA RESEARCH AND DEVELOPMENT CENTER

NOTICE

This report was prepared as an account of Government sponsored work. Neither the United States, nor the National Aeronautics and Space Administration (NASA), nor any person acting on behalf of NASA:

A.) Makes any warranty or representation, expressed or implied, with respect to the accuracy, completeness, or usefulness of the information contained in this report, or that the use of any information, apparatus, method, or process disclosed in this report may not infringe privately owned rights; or

B.) Assumes any liabilities with respect to the use of, or for damages resulting from the use of any information, apparatus, method or process disclosed in this report.

As used above, "person acting on behalf of NASA" includes any employee or contractor of NASA, or employee of such contractor, to the extent that such employee or contractor of NASA, or employee of such contractor prepares, disseminates, or provides access to, any information pursuant to his employment or contract with NASA, or his employment with such contractor.

Requests for copies of this report should be referred to

National Aeronautics and Space Administration
Office of Scientific and Technical Information
Attention: AFSS-A
Washington, D.C. 20546

NASA CR-54544
PWA FR-1713

SINGLE STAGE EXPERIMENTAL EVALUATION OF SLOTTED ROTOR AND STATOR BLADING

PART I - ANALYSIS AND DESIGN

PREPARED FOR
NATIONAL AERONAUTICS AND SPACE ADMINISTRATION
CONTRACT NAS3-7603
27 July 1966

CONTRACTOR PROGRAM MANAGER: Charles G. Linder
CONTRACTOR PROGRAM ADVISOR: Burton A. Jones

TECHNICAL MANAGEMENT
NASA LEWIS RESEARCH CENTER
CLEVELAND, OHIO

NASA PROGRAM MANAGER: John E. McAulay
Air Breathing Engines Division

NASA RESEARCH ADVISOR: L. Joseph Herrig
Fluid Systems Components Division

Pratt & Whitney Aircraft
FLORIDA RESEARCH AND DEVELOPMENT CENTER
DIVISION OF UNITED AIRCRAFT CORPORATION
UA®

ABSTRACT

31938

A program was initiated to establish the feasibility and extent to which slotted blade concepts can be utilized to increase the allowable blade loadings and stable operating range of subsonic compressor stages. As part of this program, analysis and design of the hardware required were made. Vector diagrams for three slotted rotors with tip diffusion factors of 0.53, 0.59, and 0.70 and three slotted stators with hub diffusion factors of 0.60, 0.67, and 0.76 were established. These blade rows, along with supporting hardware such as a flow generation rotor and wall bleed system, were then designed.

Author

CONTENTS

ILLUSTRATIONS

ILLUSTRATIONS (CONTINUED)

SECTION I
SUMMARY

A program has been initiated to establish the feasibility and the extent to which slotted blade concepts can be utilized to increase allowable blade loadings and stable operating range of compressor stages. Three slotted rotor and three slotted stator blade row configurations will be tested individually. The slotted rotor configurations will each be tested with the same unslotted stator blade row, and the slotted stator configurations will be tested with a representative state-of-the-art flow generation rotor. The most favorable slotted rotor and stator configuration as determined from the above tests will be combined as a complete stage to evaluate interaction effects.

The analysis and design effort for this program is discussed in this report. Vector diagrams were selected and slotted blading (65-series airfoils) was designed to provide three sets of rotors with rotor tip diffusion factors of 0.53, 0.59, and 0.70 respectively, and three sets of stators with stator hub diffusion factors of 0.60, 0.67, and 0.76. The corresponding design inlet relative Mach numbers are 0.81, 0.83, and 0.78 for the rotor tip sections, and 0.644 at the hub for all three stator configurations. A flow generation rotor and four sets of inlet guide vanes were designed to provide the necessary inlet conditions and to permit stage operation of any combination of rotor and stator.

An abbreviated annular cascade slotted stator test program and a boundary layer analysis were performed to provide preliminary slot geometry and location design information for the single stage blading. Rotor blade slots were located at 50% chord and stator slots were located at 55% chord. The slots were sized according to the ratio of slot to total flow estimated for the cascade test configurations modified by a loading parameter.

A boundary layer bleed system design was provided for the P&WA test rig in accordance with program requirements. Stress and vibration analyses and exploratory tests were performed for the blading and the test rig to determine and to eliminate or avoid areas of potentially critical operation. It was determined that slots do not adversely affect blade fatigue life if properly designed and fabricated.

SECTION II
INTRODUCTION

Advanced airbreathing propulsion systems require lightweight compact compressors capable of high performance. These compressors must have a wide range of operation, and a large stall margin, and should be insensitive to inlet flow distortion. Advance in compressor technology has been evidenced by continual increases in rotor speed, stage loading or D-factor, and reduction in stage length. Although further improvement is possible through optimizations and improved combinations of the above parameters, severe aerodynamic and mechanical limitations (such as increased losses and decreased stall margin) are imposed as a result of arbitrarily extending any one of these parameters beyond current design practice. It appears, therefore, that significant advancements in compressor technology require (1) advanced rotor and stator concepts in terms of improved blading for high flow Mach numbers, (2) high lift devices for stators and rotors, and (3) a more adjustable geometry to extend the stall-free flow range. Progress in any of these areas may result in a sizable reduction in the number of compressor stages required for any specific application, and an improved compressor.

An experimental program was initiated to investigate the application of high lift devices (in the form of slots) to rotors and stators. Isolated airfoil and wing theory experience has shown that the use of high-lift devices, such as slots, may increase the lift/drag ratio of the airfoil. Preliminary work in the jet engine field has indicated that compressor range and efficiency can be increased through the use of slots. In the present program, an investigation of slots will be made to establish the feasibility and extent to which slotted blade concepts can be utilized to increase allowable blade loadings and the stable operating range of compressor stages. A secondary objective is to collect blade element data for design use. To accomplish these objectives, three stator blade rows and three rotor blade rows of different loading levels will be built and tested individually. In the test with stators, a representative state-of-the-art rotor will be used to generate the stator inlet flow. After completion of the tests of slotted rotor and stator blades, the most favorable configuration of each will be put together and tested as a complete stage to evaluate interaction effects.

The purpose of this report is to present the objectives and results of the design effort for the slotted blading and the single stage test rig. Three rotors, three stators, a flow generation rotor, and four inlet guide vanes were designed. A vector diagram analysis was performed to choose sets of velocity diagrams for the rotors and stators over a range of loading that is beyond the loading levels associated with current design practice for state-of-the-art compressors. The rotors were designed to provide constant stator inlet conditions to allow any rotor to be tested with any stator.

A survey of the literature on slotted airfoils indicated that no useful data or design criteria were available for the application of slots to turbomachinery (airfoils in cascade at relatively high Mach numbers). Therefore it was decided to conduct a preliminary annular cascade investigation* of slotted stators to determine, in general, a preferred slot geometry and location for the test rotors and stators. Although the annular cascade program was limited in scope, it was extremely useful in the selection of slot geometry and location, and the results indicated a definite potential of slots for compressor performance improvement. The results of the annular cascade program were combined with a boundary layer separation analysis to determine slot locations for the test blading.

The investigation of slotted rotors and stators will be conducted in a single-stage compressor test rig that was designed and built by Pratt & Whitney Aircraft for the evaluation of advanced compressor concepts. This test rig meets the overall design objective, which was to provide an environment for a stage that is similar to the middle stage of a state-of-the-art compressor. Screens for producing radial and circumferential distortions were also designed. A description of the test rig and the associated test facility equipment is included in the mechanical design section of this report.

---

*The results of this investigation will be presented in a subsequent report.

As part of the overall design effort, a detailed evaluation was made of blading and test rig stress and vibration characteristics. Exploratory fatigue life tests were conducted with representative slotted blades to determine the effect of slots on vibration and fatigue strength characteristics. The effect of slots on flutter characteristics was also investigated. Finally, various methods for the fabrication of the desired slot geometries in the test blading were evaluated.

SECTION III
AERODYNAMIC ANALYSIS AND DESIGN

A. DESIGN REQUIREMENTS

1. General Stage Requirements

In general, the aerodynamic design objective was to provide (1) a stage design representative of an advanced compressor middle stage and (2) blading designs suitable for the evaluation of rotor blade and stator slots at selected loading levels beyond the current state-of-the-art.

Specific design requirements for the stage are listed below.

1. Blading will be designed according to the following:
   a. Three rotors, three stators, a flow generation rotor, and necessary inlet and exit guide vanes
   b. Compatibility of the blading profile shapes with the slotted blading concept, and compatibility of all rotor and stator combinations
   c. Aspect ratio not less than 2.0 unless otherwise dictated by mechanical design considerations, but in no event less than 1.0
   d. Solidity representative of current design practice
   e. Slotted blading performance to be estimated in terms of incidence angle, deviation angle, and loss
   f. Guide vane turning should be within current design practice to ensure that no flow blockage problems occur.
2. An existing test rig, available for this program, will accommodate a required rotor tip diameter of approximately 40 inches. The rig is designed so that blade stagger adjustments and stage changes can be accomplished on the test stand.
3. Provisions for wall bleed will be made on the inner and outer shrouds of the stator rows and on the outer casing of the rotor rows.

4. Blade vibrational characteristics and other operational conditions will be studied to assure mechanical reliability.

2. Slotted Stator Stage Requirements

The following aerodynamic analysis and design requirements were specified for the slotted stators.

1. Stator hub loading should cover the range between slightly above the upper level of current design practice (D-factor ≈ 0.60) and an arbitrary higher upper limit (D-factor ≈ 0.75).

2. All stators should be designed with the same inlet conditions for compatibility with the flow generation rotor and slotted rotors.

3. Stator inlet Mach number should be consistent with the upper level of design practice for the airfoil series selected, and should not exceed the critical value. (Because the 65-series airfoil was being considered for stator blading, a stator hub Mach number of approximately 0.65 was selected.)

4. Stators should not turn the flow beyond the axial direction.

5. The flow generation rotor (1) should be conservatively loaded to ensure a stable profile at the stator inlet, (2) should not turn the flow beyond the axial direction to ensure stable operating characteristics, and (3) should have a design tip speed within current design practice.

3. Slotted Rotor Stage Requirements

The following aerodynamic analysis and design requirements were specified for the slotted rotors.

1. Exit conditions for all rotors should be such that they match the standard inlet condition determined for the stators. Thus, any rotor can be tested with any stator.

2. Rotor tip loading levels should bracket the range from slightly beyond the level of current design practice (D-factor ≈ 0.50) to an arbitrary upper limit (D-factor ≈ 0.70).

3. Rotor tip relative Mach numbers should be kept to the levels of current design practice for 65-series airfoils ($M \approx 0.8$).

B. VECTOR DIAGRAM ANALYSIS

1. Slotted Stators

The vector diagram analysis for the stators is illustrated graphically in figures III-1 and III-2. Figure III-1 shows stator hub D-factor as a function of stator inlet and exit angle. The range of interest on this plot with respect to the specified design requirements is indicated by the shaded areas. Figure III-2 shows flow generation rotor tip D-factor as a function of inlet guide vane swirl for values of stator hub inlet angle corresponding to the limits shown in figure III-1. The region of interest on this plot is also indicated by the shaded area. The values of constant rotor turning were determined as the limiting values for this region of interest. The objective of the analysis was to determine the guide vane swirl angle (distribution) and the stator inlet angle (distribution) combination that satisfied both the rotor and stator loading and the Mach number requirements, and resulted in the compatibility of all rotor and stator configurations. It was found in the analysis that a nearly constant stator inlet flow angle, leading to a simple stator shape, could be attained without any penalty in predicted performance.

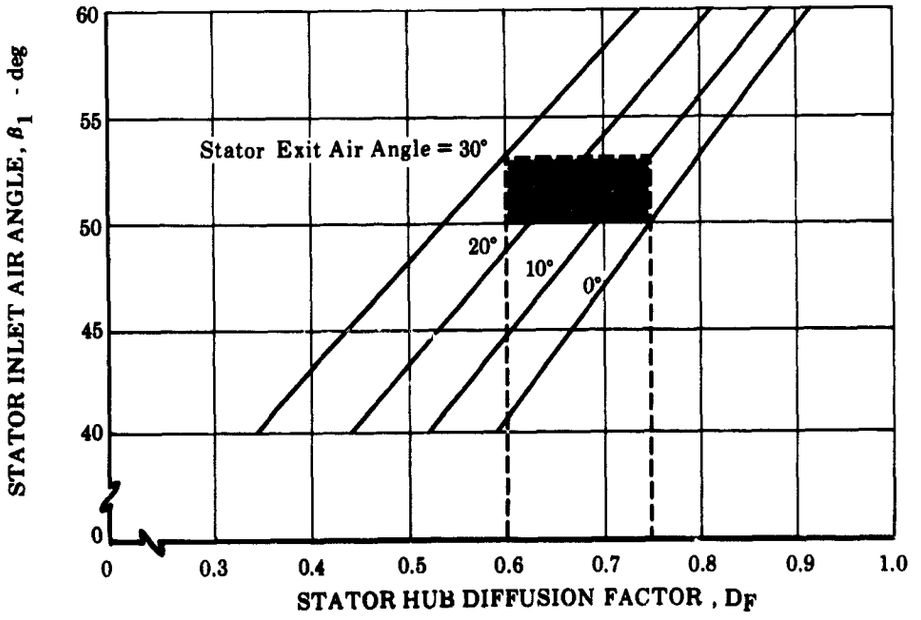

Figure III-1. Variation of Stator Hub Loading with Inlet and Exit Air Angle FD 14731

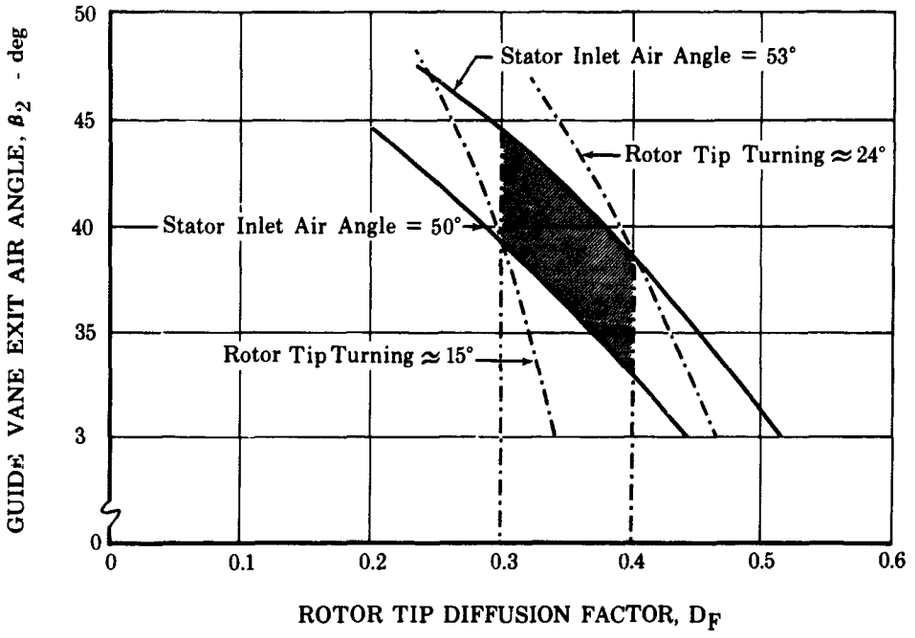

Figure III-2. Variation of Flow Generation Rotor Tip Loading with Guide Vane Exit Air Angle FD 14732

The data required to generate curves similar to those in figures III-1 and III-2 were obtained by means of a computer program. (Computer programs used in the analysis and design effort are summarized in Appendix C.) Values of wheel speed and weight flow, estimated for the initial calculations, were used for the computer calculations. Several values of inlet guide vane swirl angle (distribution) were evaluated with different levels of rotor turning and stator exit angle selected from within the predetermined ranges of interest. The computer program provided numerical solutions of the velocity triangles at 11 spanwise locations at each axial station.

The results of the initial computer calculations permitted determination of definite values of inlet guide vane swirl and stator inlet angle. Further calculations were performed with minor adjustments to swirl distribution and wheel speed to achieve the desired Mach number levels at the rotor tip and stator hub. Velocity triangles for the three slotted stator stages are presented in figure III-3. Vector diagram data for the inlet guide vane, flow generation rotor, and three slotted stator configurations are presented in Appendix B (tables B-1 through B-5). Vector diagram data for unslotted stators are included for comparisons.

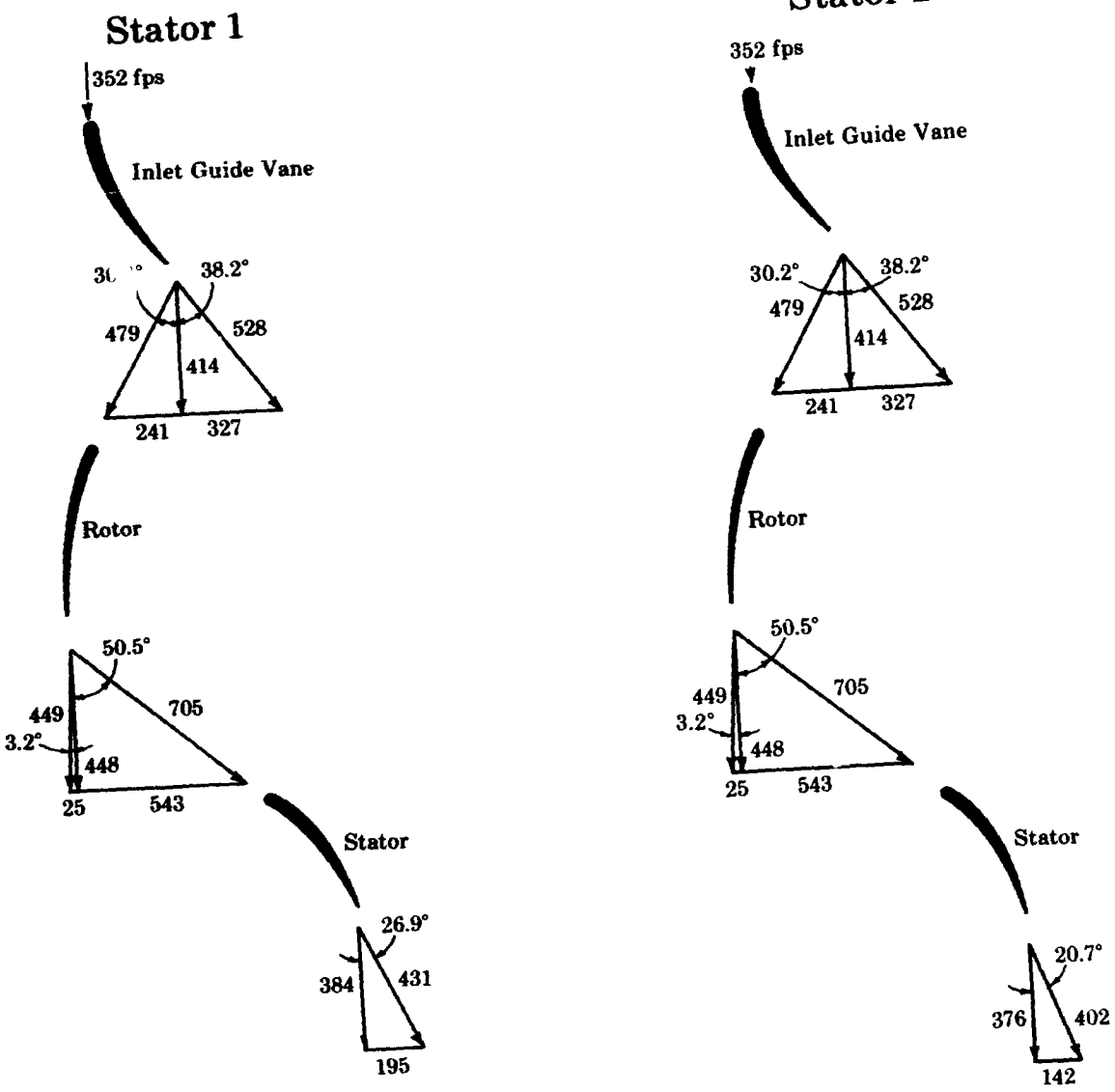

FD 15353

Figure III-3. Slotted Stator Velocity Triangles, 90% Span (from Tip)

2. Slotted Rotors

The slotted rotor analysis was concerned with the definitions of velocity triangles for three inlet guide vane configurations and three slotted rotor configurations. The problem for the slotted rotors was similar to that of the flow generation rotor. A curve of diffusion factor as a function of inlet guide vane swirl angle was generated for the stator inlet angles determined previously, as shown in figure III-4. The region of interest is identified by the shaded area in the figure. It was found that one rotor speed and flow rate would not satisfy all of the specified rotor and stator requirements. Consequently, several values of flow and speed were evaluated at each loading level.

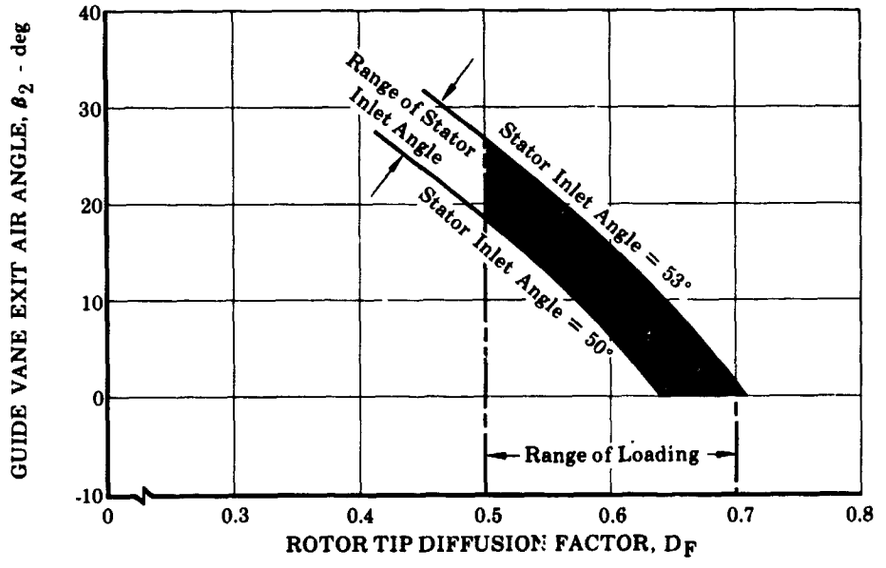

Figure III-4. Variation of Slotted Rotor Tip Loading with Inlet Guide Vane Exit Air Angle FD 14730

Velocity triangles selected for the three slotted rotor stages are presented in figure III-5. Vector diagram data for the three inlet guide vanes and three slotted rotor configurations are presented in Appendix B (tables B-6 through B-11). Vector diagram data for unslotted rotors are included for comparison. In addition, the design weight flow and rotor speed are listed for each rotor.

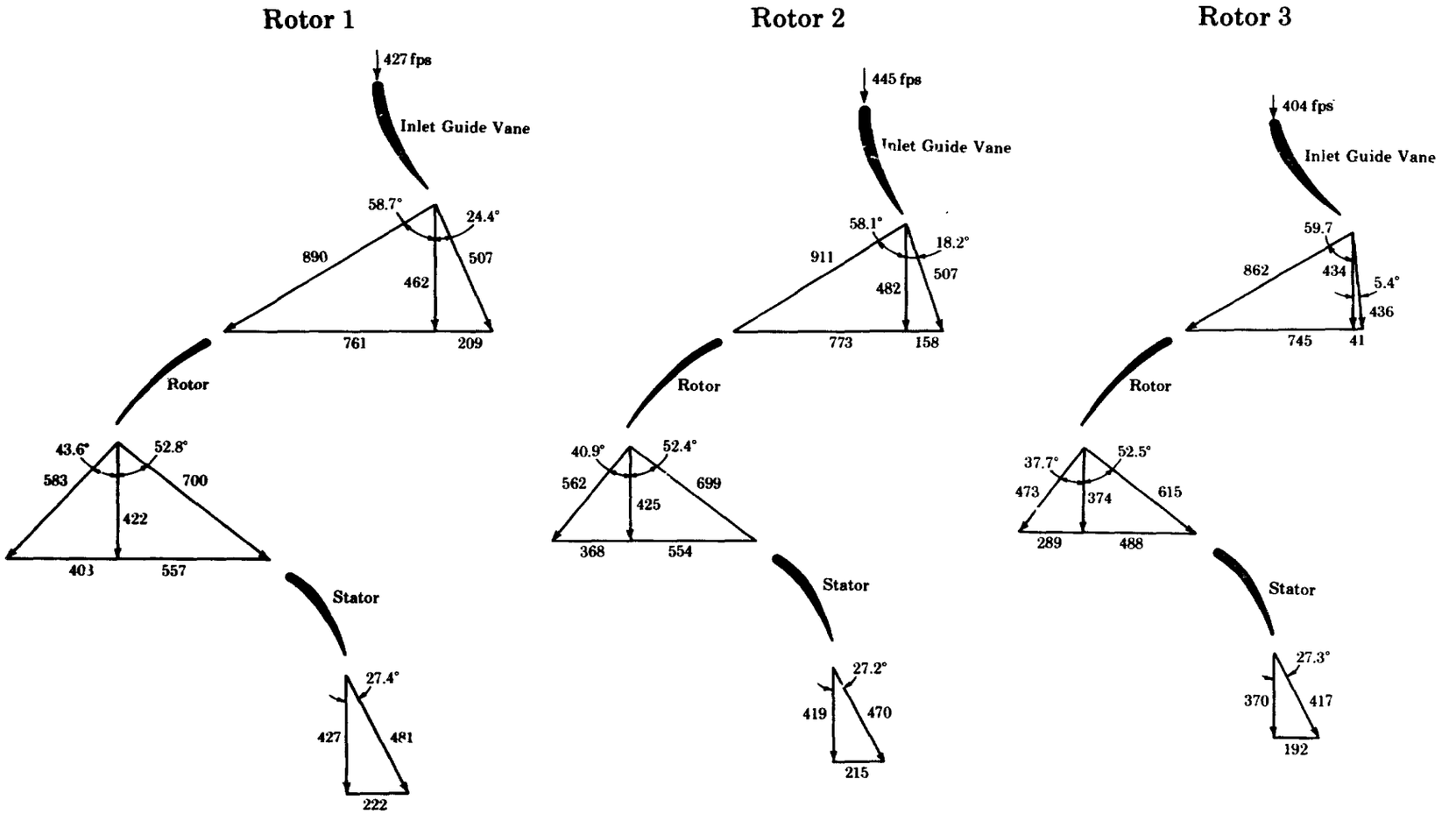

Figure III-5. Slotted Rotor Velocity Triangles, 10% Span (from Tip)

FD 15354

C. STAGE AERODYNAMIC DESIGN

1. Airfoil Series Selection

The 400-series airfoil was selected as the inlet guide vane airfoil for use with the three slotted rotors because it is suitable for the comparatively low turning requirements and a great amount of data is available from past use of this guide vane airfoil in compressors. The inlet guide vane for use with the flow generation rotor has a high turning requirement, and consequently the 63-series airfoil was chosen because it gives high turning efficiently and has less chance of limiting the airflow.

The 65-series airfoil was selected for the rotors, the stators, and the exit guide vane. This series airfoil was selected because it has adequate thickness for slots, a suitable loading distribution, and is capable of operating in the required Mach number range. In addition, Pratt & Whitney Aircraft has a large amount of cascade data and compressor development experience with the 65-series airfoil thus offering a sound basis for evaluation of the effectiveness of slots. Because of the absence of design data for slotted airfoils as applied to turbomachinery blading, it was not considered wise to attempt to develop analytically a more applicable thickness distribution or mean camber for the selected airfoil shapes. The basic blade profiles of the three airfoil series chosen for this program are shown in figure III-6.

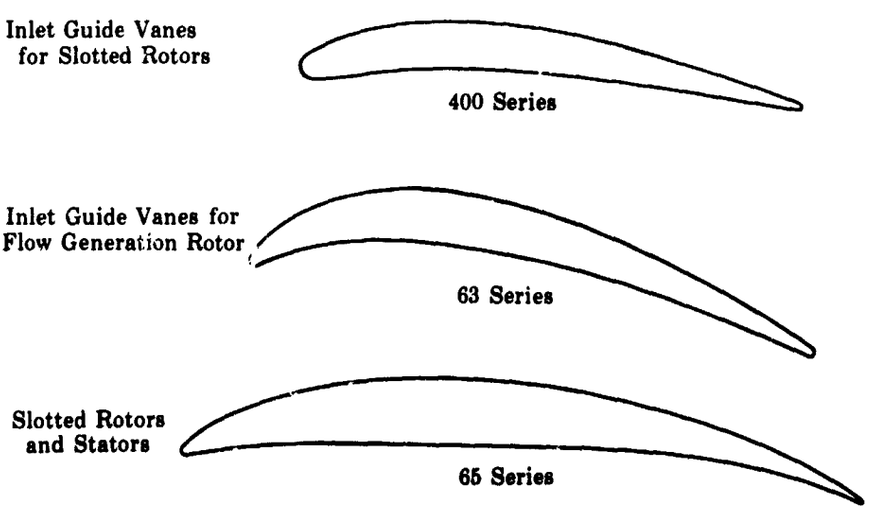

Figure III-6. Selected Airfoil Series FD 14702

2. Blading Design Parameters

Solidity, thickness ratios, and aspect ratios for the selected series airfoils are approximately the same as those of a representative middle stage of an existing state-of-the-art compressor.

Rotor and stator blading trailing edge metal angles (K_2) were determined on the basis of the assumption that slots would reduce NASA standard deviation by 50%. Incidence angles correspond to near-minimum loss values over the blade span. To reduce fabrication complexity and to provide better dimensional tolerance control, the stators and the exit guide vane were designed with constant chord and constant camber. This was possible because the stator inlet flow angles were nearly constant, as noted earlier.

A summary of blade element geometry design parameters for all blading is presented in Appendix B (tables B-12 through B-22). The design data are given at five spanwise locations, at approximately 10, 30, 50, 70, and 90% span. The following parameters are tabulated: airfoil series, chord, solidity, camber, leading and trailing edge metal angles, incidence angle, throat-to-critical area ratio, deviation, loss, thickness ratio, and aspect ratio.

3. Flow Path

The flow path for the test rig was designed to resemble the middle stage of a state-of-the-art compressor. This design, in conjunction with the selected blading design, provided the desired Mach number conditions, and is consistent with the specified diameter and hub/tip ratio requirements. To facilitate easier fabrication, regions of low wall divergence were maintained as straight wall sections. A layout of the flow path, with pertinent axial dimensions and diameters indicated, is shown in figure III-7.

The flow path entrance section consists of a bellmouth inlet and slightly converging walls through the support strut region to the inlet guide vane station. Thereafter, the inner diameter is constant and the outer diameter decreases very slightly to the stator exit. The diameter at the rotor tip is 40.4 inches and the hub/tip ratio is 0.804 at the rotor inlet.

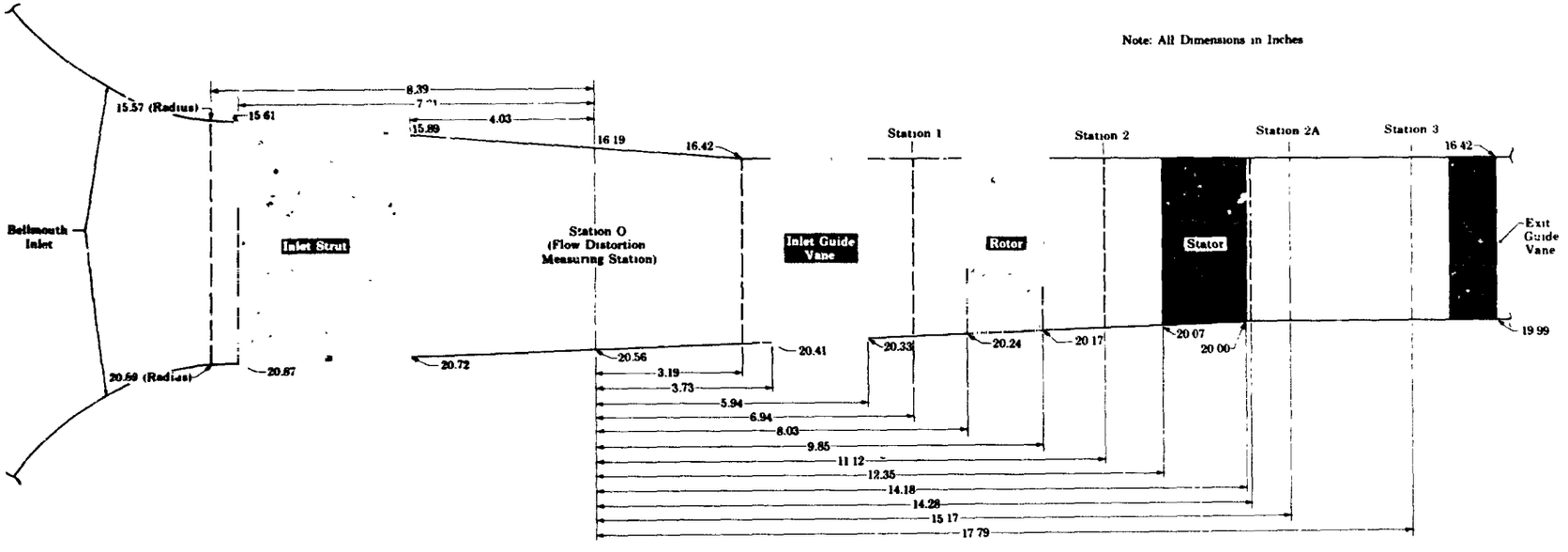

Figure III-7. Flow Path

FD 14685

4. Bleed System

To lessen the possibility of flow separation from the wall due to excessive boundary layer buildup, wall bleeds on the inner and outer shrouds of the stator row and on the outer casing over the rotor blade tips have been provided. Figure III-8 shows details of the bleed system. Air is bled from the walls through perforated plates into cavities at the blade tip and at the stator root and tip. These cavities (or manifolds) are connected to the second-stage test stand ejector with separate rotor and stator control valves and flow measuring orifices. The ejector inlet pressure design point was established at 5 psia, and the perforated shrouds were sized for approximately 5% total bleed at design flow conditions. Analysis of the flow through the perforated shrouds, which have a hole diameter of 0.078 inch and a 5% area opening, indicated a Mach number of 0.25 through the holes and a maximum shroud deflection of 0.002 inch due to the pressure differential across the sheet. Rotor tip clearance is 0.040 inch and the calculated rotor tip growth at maximum speed conditions is 0.024 inch.

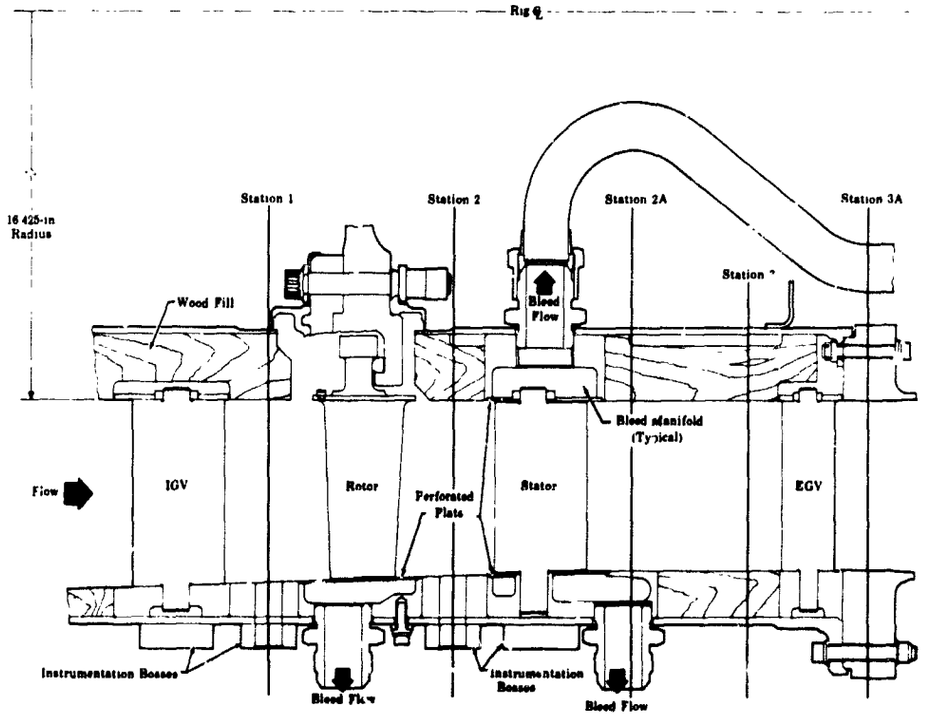

Figure III-8. Rotating Cascade Rig Bleed System FD 14683

This method resulted in geometrically similar slot configurations for the rotating rig rotor and stator blading. Aside from general geometric similarities, the two most important criteria for slot design are considered to be (1) the slot exit flow angle relative to the suction surface and (2) the percentage slot flow. Further refinements to scaling techniques should be considered in the future. For example, it should be determined whether slot flow energy ($\sim V^2$) or momentum ($\sim V$) is of primary importance. This type of refinement can be investigated in systematic annular cascade tests.

2. Slot Location

General criteria for the slot location on a heavily loaded compressor blade or stator were established as follows:

1. The slot should be located upstream of the point of flow separation. If the slot flow is exhausted into a separated region it cannot effectively turn the primary flow back toward the suction surface.

2. The slot should be located in a region where the pressure difference between suction and pressure surface is sufficiently high to provide high slot flow velocity. High slot flow energy is important to permit sufficient energy addition to the suction surface boundary layer for unseparated flow essentially to the blade trailing edge.

From the annular cascade test program, it was learned that a slot at 55% chord was more effective than a slot at 75% chord relative to boundary layer separation at approximately 85% chord and minimum pressure point at 23% chord. For lack of a better criterion, it was decided to maintain this relative slot location for the rotating rig blading. Thus, the slot would be located approximately halfway between the minimum pressure point and the separation point*. This criterion is generally consistent with the criteria listed above.

---

*$\frac{0.55 - 0.23}{0.85 - 0.23} = 0.516$

The major problem of determining slot locations for the rotating rig blading was therefore one of predicting the flow separation point for the three rotor and three stator configurations. This was accomplished by applying boundary layer separation criteria for flow over a curved surface in an adverse pressure gradient.* This presentation defined a limiting pressure rise (in terms of velocity) for a given Mach number, Reynolds number, and momentum thickness at the minimum pressure point, and length of pressure rise, L. For minimum pressure point Mach numbers greater than 1.0, or Reynolds number greater than 10^6, the equation for limiting energy recovery (pressure rise) is

$$E_{LIM} = 1 - \left(\frac{V_s}{V_{s_{max}}}\right)^2 = 1 - 3.24\left(\frac{\theta}{L}\right)^{0.324}$$

For initial Mach numbers less than 1.0 and Reynolds numbers less than 10^6,

$$E_{LIM} = 1 - \left[0.053\left(\frac{\theta}{L}\right)^{-0.81}\right] - 2\left[0.075\left(R_\ell \times 10^{-6}\right) + 0.125\right]$$

The momentum thickness (θ) is obtained from the Blasius equation for laminar flat-plate flow

$$\theta = 0.664\ell \Big/ \sqrt{R_\ell}$$

where ℓ is the distance from leading edge to the minimum pressure point. Experimental data show that this equation offers a good approximation of the momentum thickness for flow over a curved surface in a favorable pressure gradient.

Values of limiting energy recovery were calculated for several lengths of pressure rise to establish a distribution of limiting energy recovery in the chordwise direction. These calculations were performed for both root and tip conditions. The resulting values were compared with those determined from theoretical pressure coefficient distributions, corrected for compressibility, using the Karman-Tsien correction. The point of separation was considered to be the chordal location of the intersection of these two energy recovery distributions; a typical case is shown in figure III-13.

*Reference: Jones, B.A., "Method for Prediction of Boundary-Layer Separation and Growth for Application to Turbine Blade Design," presented at ASME Fall Meeting, Hartford, Connecticut, September 23-25, 1956.

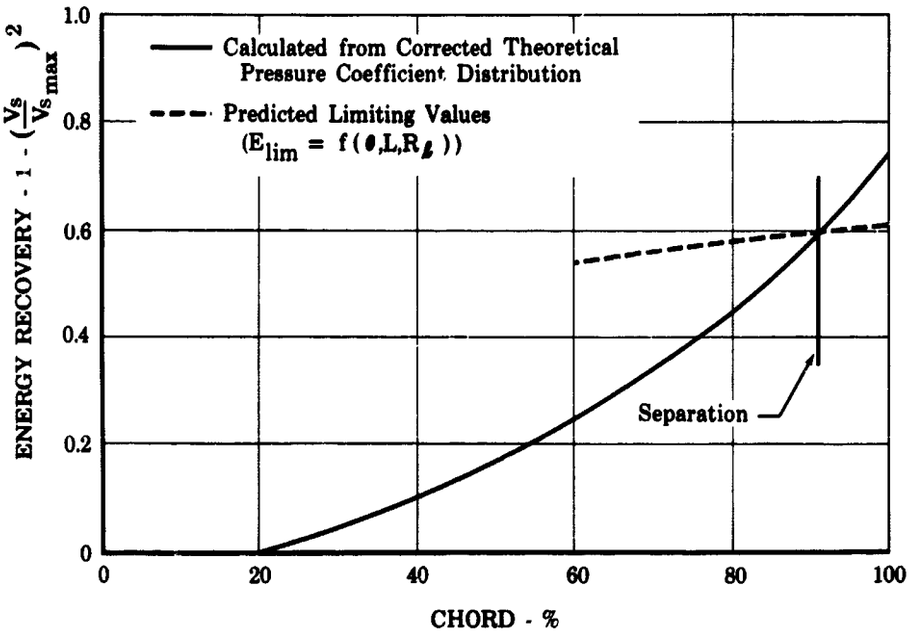

Figure III-13. Energy Recovery Distribution - Rotor 1, Root Section FD 14706

Where the local Mach number exceeded 1.0, an equivalent normal shock pressure rise was assumed to occur over 5% chordal distance downstream of the minimum pressure point. A typical case (rotor 2, root section) is shown in figure III-14. The chordwise separation points thus determined for the root and tip sections of the three rotor and stator configurations are as follows:

	Predicted Separation Point	
Rotor	Root (90% Span)	Tip (10% Span)
1	0.91	Possible shock separation
2	0.91	Not separated
3	0.80	Not separated
Stator		
1	0.96	0.95
2	0.93	0.94
3	0.91	0.89

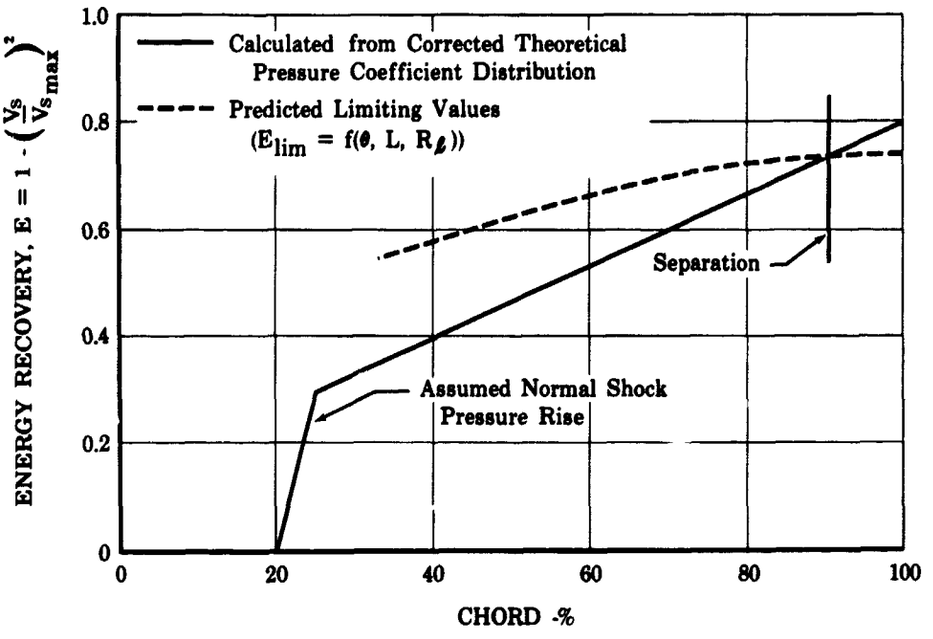

Figure III-14. Energy Recovery Distribution - Rotor 2, Root Section FD 14707

The next step in the procedure was to relate predicted separation points to observed separation points, and apply any differences to the predicted points. Observed separation points were available from the annular cascade test results. A comparison of the predicted and measured values for two annular cascade stator configurations is shown below:

	Predicted Separation Point	Observed Separation Point
First stator (nominal incidence)	0.95	0.85
Second stator (high incidence)	0.74	0.67

The differences between predicted and observed separation points were used to determine an adjustment factor, as follows:

$$S_a = \frac{SP_{predicted} - SP_{observed}}{SP_{predicted}}$$

where:

S_a = adjustment factor

SP = separation point.

Values of this factor were calculated for the two annular cascade stators, and are shown plotted in figure III-15. Assuming a linear distribution for the region of concern (between about 70 and 100% chord), it is possible

to estimate the probable separation points for the rotating rig blading. These probable separation points are as follows:

Rotor	Probable Separation Point: Root (90% Span)	Probable Separation Point: Tip (10% Span)
1	0.82	Possible shock separation
2	0.82	Not separated
3	0.72	Not separated
Stator		
1	0.86	0.85
2	0.83	0.84
3	0.82	0.80

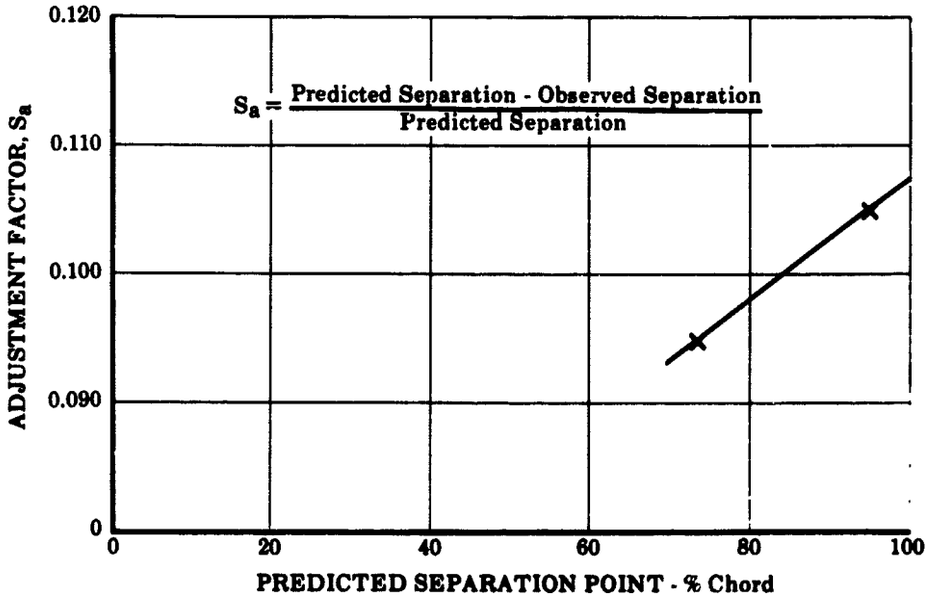

Figure III-15. Separation Point Adjustment Factor Values FD 14704

Applying the criterion for slot location relative to minimum pressure and separation points (see the beginning of paragraph D.2) results in the following slot locations (where separation was not indicated, a percent chord value of 1.0 is used).

SECTION IV
MECHANICAL DESIGN

The mechanical design work performed under this contract consisted of the design of (1) compressor blading, (2) associated test hardware, and (3) a boundary layer bleed system. As part of the design effort, a study was conducted to determine the effect of slots on blade vibration and fatigue characteristics.

Although the test rig and drive system were not designed and fabricated under the contract program, a description of the rig including pertinent mechanical design information is presented.

A. BLADING DESIGN

1. Steady-State Stress Analysis

a. Airfoil

All rotor blade, stator, and inlet guide vane configurations were analyzed to determine stresses due to centrifugal loads and/or gas bending loads. A computer program that calculates blade element airloads and section properties at 11 radial stations was used in the analysis. Airloads were integrated spanwise, and airfoil section properties were linearly faired to mathematically reproduce the relationship between fluid forces and blade geometry. Gas bending stresses were calculated at the leading and trailing edges and on the convex surface at the point of maximum thickness. The restoring effect of the centrifugal forces that tends to reduce gas bending stresses was considered in the rotor stress analysis. The net gas bending stress and centrifugal tensile stress were added to yield the total blade stress. The rotor and stator configurations that had the highest calculated stress level were reevaluated with a slot that extended from approximately 5 to 95% span and located at the 50% chord position. The results of this analysis are given in table IV-1. As shown in the table, the steady-state blade element stresses were found to be well within the design limits for the materials considered for both slotted and unslotted airfoil sections.

5. Distortion Screens

The effects of radial and circumferential inlet flow distortion on slotted compressor blading performance will be evaluated under the program. The distortion requirements are as follows:

1. Radial: outer two-fifths of the annulus area
2. Circumferential: 90 degrees of the annulus
3. Velocity distortion: $\frac{V_{max} - V_{min}}{V_{max}} = 0.232$

The velocity distortion specified above was calculated on the basis of a total pressure distortion of 0.15 at an average Mach number of 0.60. An area-average total pressure was determined for the required radially distorted profile, and the maximum and minimum velocities were subsequently calculated assuming a constant radial static pressure.

The radial distortion flow conditions for the single stage rig flow path are illustrated in figure III-9. The distortion screens are located at the inlet support strut leading edge for convenience of installation and modification. The required velocity distortion will be measured at instrumentation station 0. The distortion screen configuration was determined in the following three steps.

1. Calculate total pressure distortion at the station 0 Mach number condition (M = 0.33).
2. Assuming isentropic flow and no mixing across the two parts of the distorted profile between the screen location and station 0, calculate the equivalent velocity distortion for the Mach number condition at the screen location (M = 0.268).
3. Calculate the required screen area (height) on the basis of the predetermined flow rates in both parts of the distorted profile and the velocity distribution determined in step 2 above.

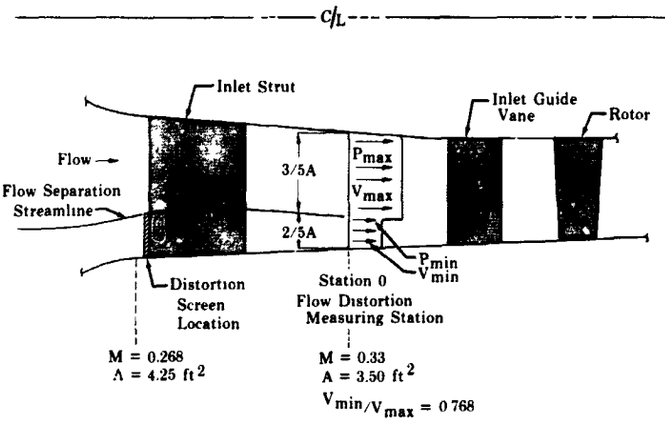

Figure III-9. Radial Distortion Flow Conditions FD 15352

The average Mach number immediately downstream of the screen was determined in the above steps, and it was assumed that this average Mach number existed immediately ahead of the screen. The calculated total pressure loss in step 1 was

$$\frac{P_{max} - P_{min}}{P_{max}} = 0.038$$

For a Mach number of 0.213 just ahead of the screen,

$$\frac{P_{max} - P_{min}}{\frac{1}{2}\rho V^2} = 1.24.$$

The screen porosity, according to data presented in NACA CB No. L5F28 for the above pressure loss and Mach number conditions, was 48%. Screen pressure drop data correlations obtained at Pratt & Whitney Aircraft resulted in porosity values of 52 and 63%. A screen porosity of 50% will be used initially.

For the circumferential distortion screens a similar analysis was made and an initial screen porosity of 50% will be used.

D. ANALYSIS AND DESIGN OF SLOTS

Slots have not previously been applied to airfoils for use in cascades at relatively high Mach numbers. It was therefore necessary to conduct an analytical and experimental program to establish both a reasonable slot geometry and a preferred slot location for investigation in the single stage rotor and stator configurations.

A series of water table tests was conducted with representative slotted vanes in cascade. Although the overall test results indicated a slight flow turning improvement with slots (about 1 degree), the use of the water table as a preliminary design tool was unsuccessful and the program was discontinued.

To investigate the effect of slot geometry variation and slot location on performance, an annular cascade program was conducted using oversize (chord) slotted airfoils. A slot geometry for the single stage rotor and stator blading was selected on the basis of test results obtained from this program. A preferred slot location relative to minimum pressure point and separation point was also determined. Boundary layer separation criteria were employed as a step in the determination of chordal locations of the slots in the single stage blading.

The methods used to arrive at slot geometry and location are discussed in the following paragraphs.

1. Slot Geometry Selection

The annular cascade program included evaluation of six slot configurations located at 55% chord and five slot configurations at 75% chord of a 6-inch chord, 65-series stator vane. All tests were conducted at approximately design incidence. Without the slots, flow separation on the suction surface occurred at approximately 85% chord as evidenced by surface pressure distribution and dye traces. The performance improvement for the 55% chord slot configurations was significantly better than that for the 75% chord slots. Performance results are presented in table III-1. The slot configurations are presented in figures III-10 and III-11, respectively, for the two slot locations. Slot configuration No. 9 in figure III-10 was selected for the compressor blading because this configuration provided the lowest wake pressure loss and the highest relative lift coefficient. (See table III-1.) It should be noted that the differences in data for several of the better 55% slot geometries are probably within the accuracy of the data.

The procedure for translation of the selected slot geometry from the annular cascade stator vane to the rotating rig blading was based primarily on maintaining geometrically similar slot configurations for different chord lengths and chordal slot locations. Slot geometry nomenclature is indicated in figure III-12.

Table III-1. Annular Cascade Slotted Stator Performance

CONFIGURATION	SLOT CHORDAL LOCATION % CHORD	WAKE TOTAL PRESSURE LOSS COEFFICIENT	LIFT COEFFICIENT
1	Unslotted	0.071	0.710
1A	Unslotted	0.068	0.680
2	55	0.023	0.665
5	55	0.021	0.716
7	55	0.031	0.762
9	55	0.012	0.768
15	55	0.014	0.716
18	55	0.030	0.707
4	75	0.063	0.765
6	75	0.053	0.732
8	75	0.073	0.744
10	75	0.130	0.661
14	75	0.125	0.705

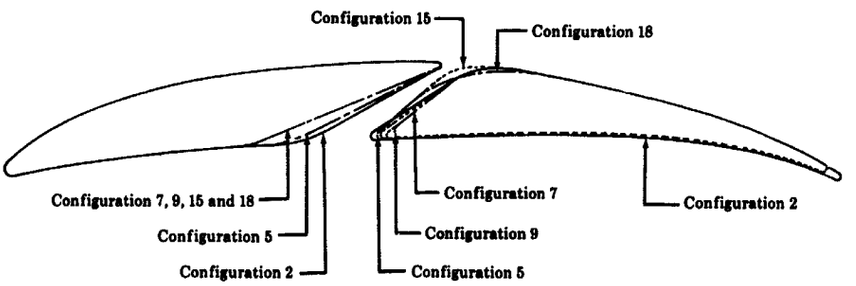

Figure III-10. Annular Cascade Stator Slot Configurations, 55% Chord Slot Location

FD 14678

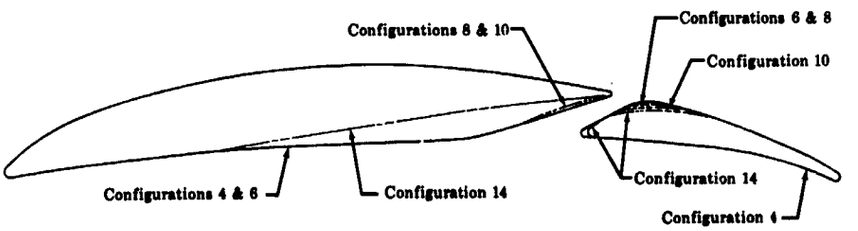

Figure III-11. Annular Cascade Stator Slot Configurations, 75% Chord Slot Location

FD 14677

Y_2 - Slot Exit Dimension, Calculated

t - Thickness at Intersection of Slot ℄ and Mean Camber Line

R - Coanda Radius, 0.792 (t)

r_1 - Slot Leading Edge, 0.097 (t)

Y_1 - Slot Capture Dimension, Determined by Translating Slope of Slot Walls from Annular Cascade Slot Configuration No. 9

r_2 - Slot Trailing Edge Radius, 0.005 in.

R_p - Pressure Surface Radius, 1.73 (t)

ψ - Angle Formed by Slot ℄ and Mean Camber Line Translated from Annular Cascade Slot Configuration No.9

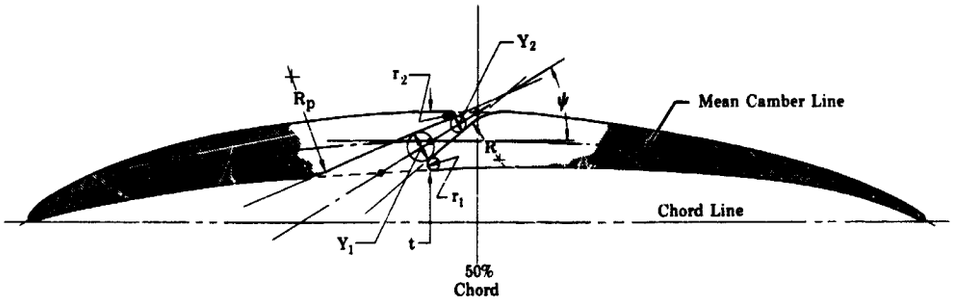

Figure III-12. Slot Geometry Nomenclature FD 14679

The first step in the translation procedure was to locate the slot centerline at angle ψ with the meanline, so that the centerline passed through the desired chordal slot location at the suction surface.

The next step was to determine the slot flow control area (Y_2 x span) for the rotating rig blading. This was accomplished by establishing two ground rules. First, for a given loading (D-factor) the rotating rig blading will have the same ratio of slot to total flow as the cascade rig blading. Second, adjustment to this flow ratio shall be made as a function of loading such that the flow ratio increases as the loading of the rotating rig blading rises. A description of the procedure used for slot sizing is given in Appendix D. With Y_2 determined, and r_2 given, the location of Y_2 (normal to the slot centerline) is fixed such that circles Y_2 and r_2 have a common point of tangency (figure III-12).

The slot side walls were located by maintaining the respective angles with the meanline that were determined from the annular cascade program. Radii, R, r_1 and R_p were then scaled according to blade thickness at the intersection of the slot centerline and the mean camber line.

Rotor	Minimum Pressure Point*		Slot Location	
	Root (90% Span)	Tip (10% Span)	Root (90% Span)	Tip (10% Span)
1	0.20	0.015	0.52	—
2	0.20	0.015	0.52	0.52
3	0.20	0.22	0.47	0.622
Stator				
1	0.33	0.30	0.60	0.58
2	0.28	0.30	0.56	0.5[illegible]
3	0.30	0.28	0.57	0.55

The average value of the chordwise separation point is 0.53 for the three rotors and 0.57 for the three stators. Because this slot location procedure is not considered to be exact, and because a slot location too far forward would be less harmful than one too far back, the slot locations were selected as 0.50 for all rotor configurations and 0.55 for all stator configurations.

*Determined from Theoretical Pressure Coefficient Distributions.

Table IV-1. Calculated Steady-State Airfoil Stresses

A. UNSLOTTED

BLADE/VANE		MAXIMUM OPERATING TEMPERATURE, °R	AMS MATERIAL DESIGNATION	0.2% YIELD STRENGTH, psi	TENSILE STRESS, psi	GAS BENDING OR NET GAS BENDING STRESS, psi	COMBINED STRESS, psi	STRESS RATIO
Inlet Guide Vane	1	560	5613	101,500	—	2,100	—	—
	2	560	5613	101,500	—	2,500	—	—
	3	560	5613	101,500	—	500	—	—
Flow Generation Guide Vane		560	5613	101,500	—	8,100	—	—
Rotor	1	617	5616	110,000	13,900	9,100	23,000	0.209
	2	624	5616	110,000	12,800	11,200	24,000	0.218
	3	623	5616	110,000	9,100	11,700	20,800	0.189
Flow Generation Rotor		583	5616	110,000	6,600	2,700	9,300	0.0846
Stator	1	624	5613	100,000	—	4,900	—	—
	2	624	5613	100,000	—	5,300	—	—
	3	624	5613	100,000	—	6,900	—	—

B. SLOTTED

Flow Generation Guide Vane		560	5613	101,500	—	5,090	—	—
Rotor	2	624	5616	110,000	12,700	8,674	21,374	0.194
Stator	3	624	5613	100,000	—	12,124	—	—

b. Blade Attachment

The desirability of adjusting blade stagger resulted in the rotor blade attachment scheme shown in figure IV-1. The cylindrical root section permits rotation of the blade, and the blade is held in place with a positioning shear pin. The cylindrical blade root section has a 0.60-inch diameter with a corresponding section modulus of more than twice that of the airfoil section modulus. Centrifugal forces and gas bending stresses due to aerodynamic loading were considered in the rotor blade attachment stress calculation. The calculations were performed for a rotor speed of 6000 rpm, which is approximately 110% of design speed. The results of stress calculations for the rotor blade attachment section are shown in table IV-2. Figure IV-1 illustrates the blade root sections that were considered for these calculations. Values of the ratio of calculated stress to yield stress, shown in the table, are within acceptable engine design limits.

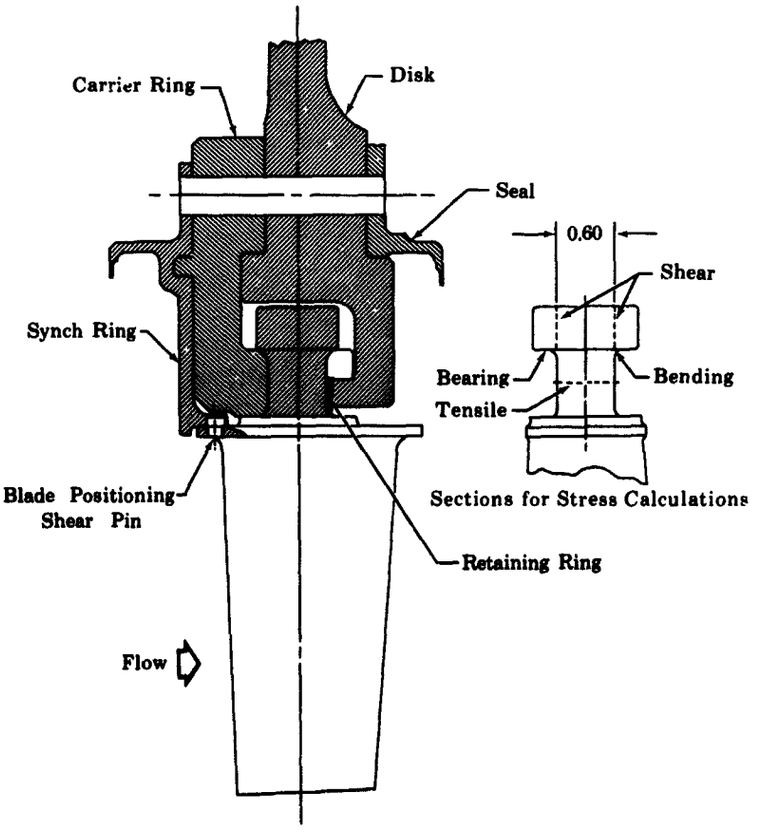

Figure IV-1. Blade Attachment FD 14705

Table IV-2. Calculated Rotor Blade Attachment Stresses

	TENSILE	BENDING	COMBINED TENSILE AND BENDING	SHEAR	BEARING
Calculated stress, psi	33,900	31,600	65,500	15,700	87,300
0.2% yield point stress, psi (AMS 5616 stainless steel)	112,000	112,000	112,000	112,000	112,000
Stress ratio	0.330	0.282	0.585	0.140	0.780

Cylindrical root (and tip) sections were also used for the guide vanes and stators, as shown in figure IV-2. The root and tip sections for the stationary blading are held in place by a fillet braze weld. The stagger of these blades is changed by heating the braze joint, repositioning, and rebrazing. The maximum bending stress due to gas loading is 29,500 psi for the stators and approximately 34,600 psi for the inlet guide vanes. This represents a satisfactory design margin for the materials indicated in table IV-1. The torsional stresses that the fillet-brazed joints will be subjected to were also calculated. The calculated stress was on the order of 2000 psi, compared to an estimated braze strength of 20,000 psi.

c. Rotor Disk

Steady-state stresses were calculated for the rotor disk and carrier ring, as shown in figure IV-1. The average tangential stress of the disk is approximately 65,000 psi at 110% of the maximum design speed, which represents a burst margin of 59% and a yield margin of 42% for the AMS 6415 material.

The carrier ring transfers the blade loads directly to the disk. The carrier ring has a tangential stress of approximately 50,000 psi at 110% of maximum design rotor speed. This provides a burst margin of 83% and a yield margin of 62%, which is well within design practice.

Bending and shear stresses were also calculated for the carrier ring at 110% of design operating speed. The bending stress was approximately 42,000 psi and the shear stress was approximately 15,900 psi. These calculated stresses are also well within design practice.

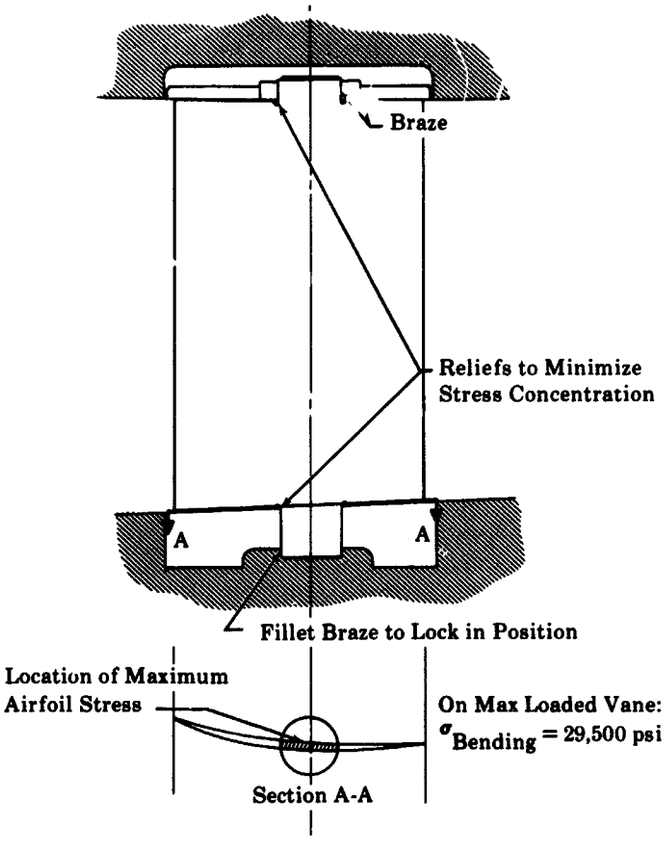

Figure IV-2. Typical Inlet Guide Vane/Stator Assembly FD 14703

Carrier ring attaching bolts were spaced four times the bolt diameter to minimize carrier ring deflection under maximum load conditions. The axial load carrying capacity of the bolts greatly exceeds the maximum operating axial load.

2. Blade Vibration and Fatigue Life Study

a. Vibration Analysis

First bending and first torsion vibration frequencies were calculated for unslotted rotors and first bending frequencies were calculated for slotted rotors and unslotted and slotted stators. The results are presented in terms of frequency versus rotor speed in figures IV-3 through IV-6. The overall range of first bending frequency for the unslotted rotors, shown in figure IV-3, is 400 to 600 cps between zero and 110% of design speed. First torsion frequency varies between about 1600 and 1700 cps at 110% of design speed. (See figure IV-4.) Lines representing

approximate factors of rotor frequency (E) are shown in the figures to permit identification of any excitation frequencies within the operating range such as inlet guide vane wakes, upstream bearing support struts, or stall zones.

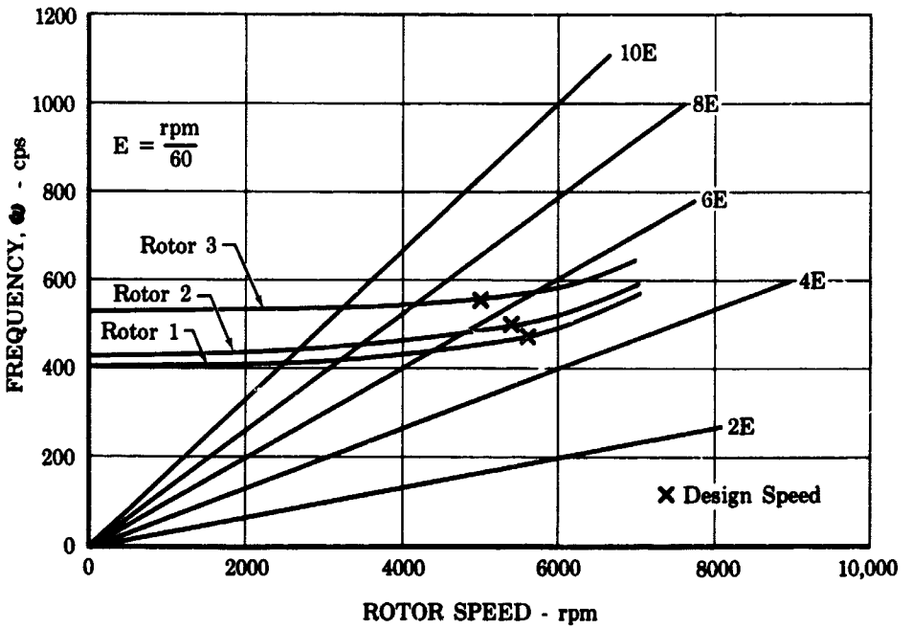

Figure IV-3. First Bending Resonance Diagram for Unslotted Rotors FD 14721

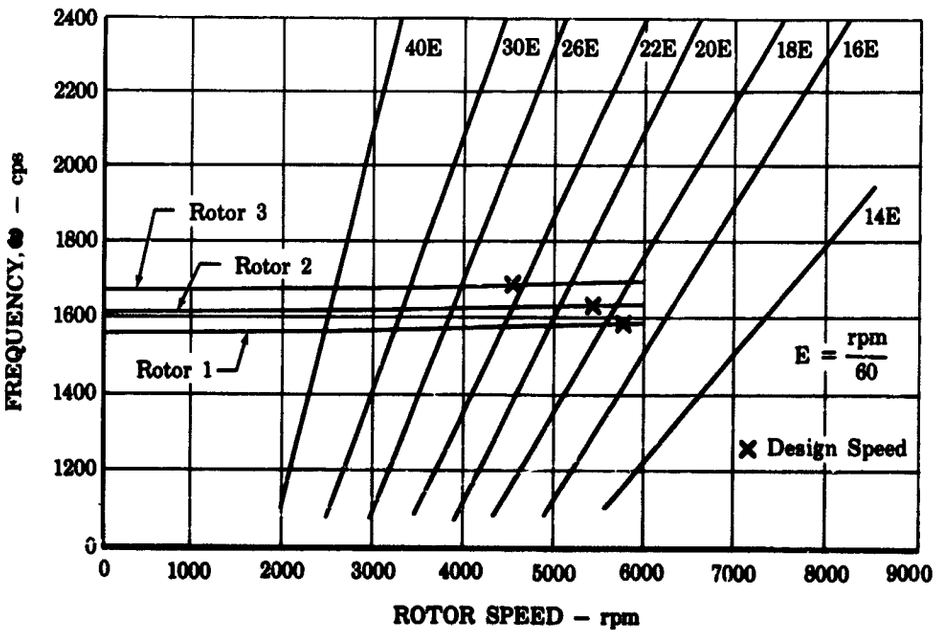

Figure IV-4. First Torsion Resonance Diagram for Unslotted Rotors FD 14722

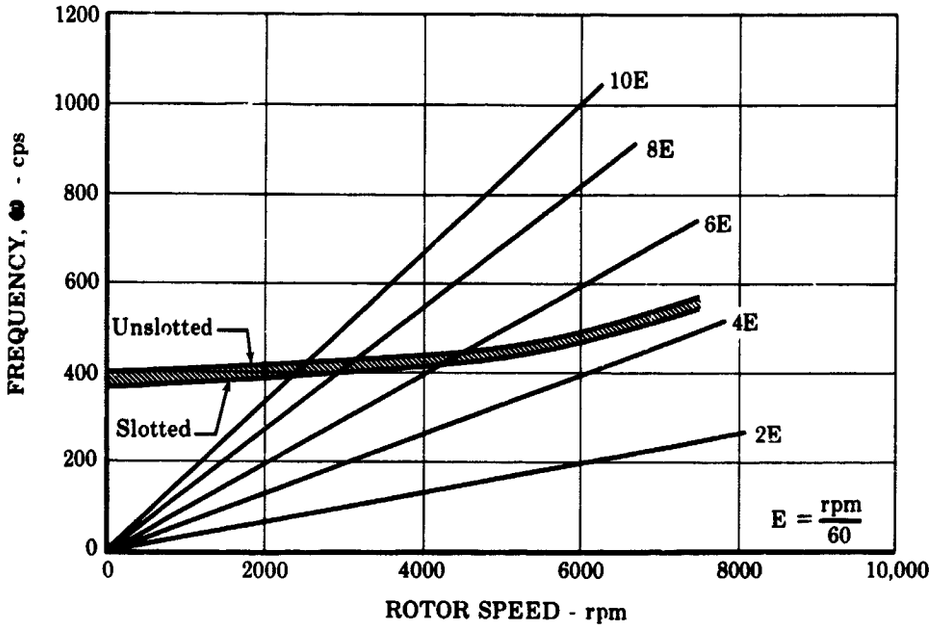

Figure IV-5. Effect of Slot on First Bending Frequency, Rotor 1 FD 14733

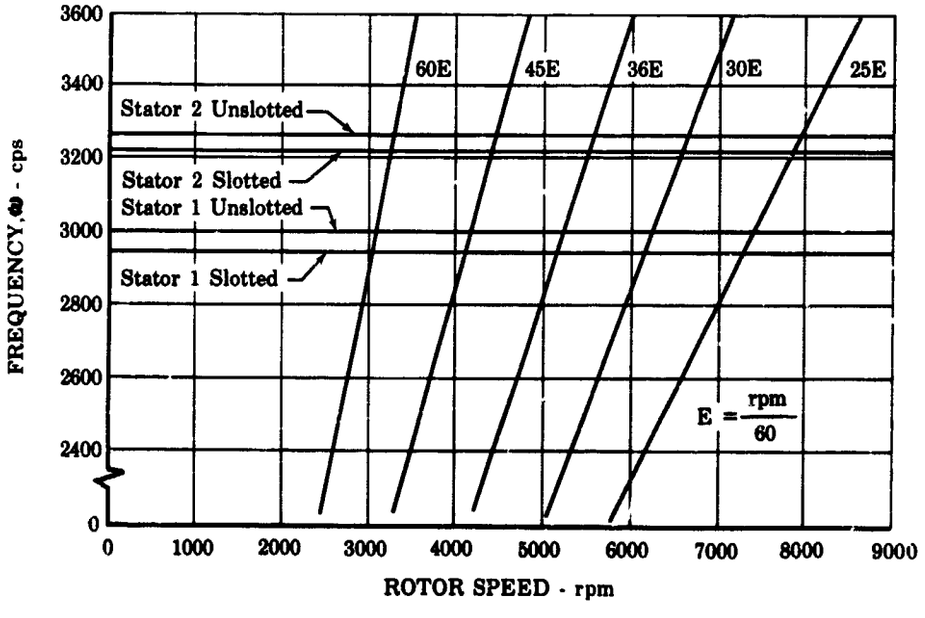

Figure IV-6. First Bending Resonance Diagram for Stators FD 14723

The effect of a slot on calculated first bending vibration frequency is illustrated in figure IV-5 for rotor configuration No. 1. Because the vibration frequency of an airfoil is proportional to the square root of the inertia-to-weight ratio, the calculated effect of the slot on vibration frequency is small.

The results of a similar analysis for unslotted and slotted stators are presented in figure IV-6 for stator configurations 1 and 2. Because the resonant frequencies are relatively high (on the order of 3000 cps), no vibration problems are anticipated for the stators.

b. Flutter Analysis

Values of flutter parameter, $K \sim \frac{V}{c\omega}$ and incidence correlation parameter were calculated for the rotors (unslotted) and compared with flutter data for 65-series airfoils as shown in figure IV-7. It is difficult to assess precisely the effect of slots on flutter characteristics. Exploratory vibration tests (discussed in a following paragraph) indicated little change in torsional frequency when a slot was added. The average decrease in frequency for a double slot* results in an increase in flutter parameter of 13%, provided that other factors remain the same. Slots appear to be effective in eliminating separation at relatively high incidence values (annular cascade results), and it is therefore probable that the flutter region indicated in figure IV-7 will be shifted upward for slotted blades. In any case, blade vibration will be carefully monitored during operation near stall.

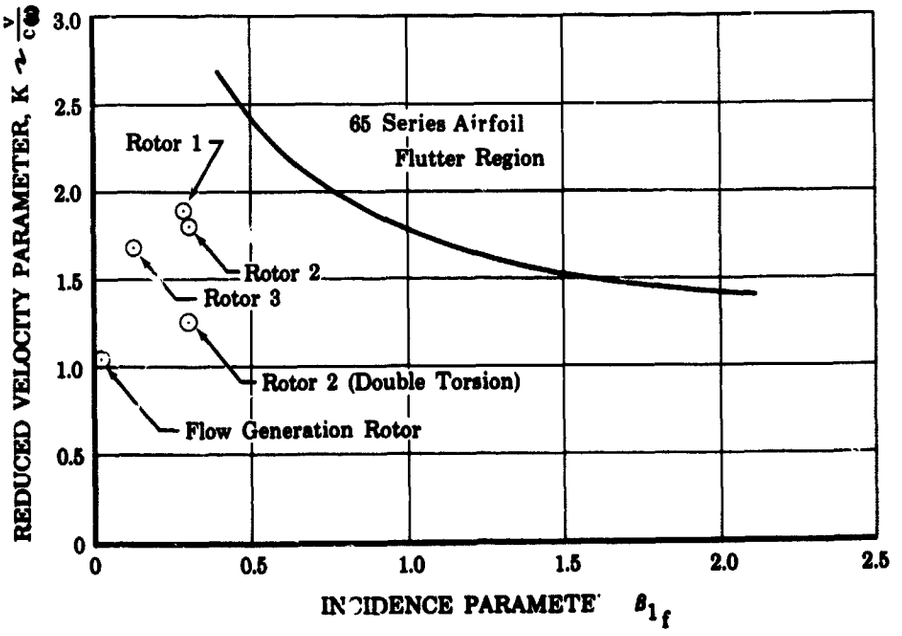

Figure IV-7. Blade Flutter at Design Conditions FD 14708

*See Table IV-4.

A particular source of concern for the slotted blading was that of double torsion (see figure E-2), resulting from the fact that the blade chord is effectively reduced by a factor of 2.0 with a mid-chord slot, thus doubling the flutter parameter value when in this particular mode of vibration. Exploratory tests conducted at the UAC Research Laboratories with representative two-dimensional blading (Appendix E) indicated that the torsional vibration frequency increased by a factor of approximately 3.0, resulting in a net reduction in the flutter parameter (see figure IV-7). It is concluded from these results that the effect of a double torsion mode of vibration will be no more serious than the flutter characteristics encountered with conventional blading.

c. Fatigue Life Tests

Exploratory tests with representative middle-stage compressor blades were conducted to determine the vibration and fatigue life characteristics of unslotted and slotted airfoils subjected to first bending and first torsion modes of vibration. Because a large number of test rotor blades were not available for fatigue life testing, existing blades of essentially the same size and geometry were used.

The fatigue life tests were performed in the following steps:

1. Determine first bending and first torsional vibration frequencies for unslotted blades, and locus of maximum stress points.
2. Determine fatigue life of unslotted blades.
3. Determine first bending and first torsion frequencies for slotted blades, and locus of maximum stress points.
4. Determine fatigue life of slotted blades.

The slotted and unslotted blade resonant frequencies are compared in table IV-3 with the calculated frequencies. Measured frequencies obtained with the representative two-dimensional blades at the UAC Research Laboratories are included for comparison. The measured frequencies for slotted versus unslotted blading generally support the calculated values.

Table IV-3. Comparison of Calculated and Measured Blade Vibration Frequencies

	1ST BENDING FREQUENCY, cps		1ST TORSION FREQUENCY, cps	
	UNSLOTTED AIRFOIL	SLOTTED AIRFOIL	UNSLOTTED AIRFOIL	SLOTTED AIRFOIL
Rotor 1 - computed values	400	370	1560	
Rotor 2 - computed values	435		1600	
Rotor 3 - computed values	525		1660	
Representative blade - test values	398 to 400	385 to 408	1370 to 1422	1140 to 1270
Flat plate (2 x 3.5 x 1/8-in.) - test values	308	310 to 312	1260	1156 to 1240

The results of the fatigue life tests are presented in table IV-4. These results were obtained by imposing bending or torsional stresses at predetermined natural frequencies starting with 25,000 psi and increasing the level in 5000-psi increments until failure occurred. The results indicate that a slot with properly rounded edges and stress relieved (glass bead peening) at the slot ends to reduce stress concentrations does not significantly affect blade fatigue life.

B. COMPRESSOR TEST RIG

The Pratt & Whitney Aircraft (FRDC) compressor research test rig, available for both the annular cascade evaluation of stator slot configurations and the single-stage evaluation of slotted blading, was designed to simulate the aerodynamic environment of a state-of-the-art compressor middle stage. Figure IV-8 shows a section view of the test rig. Design features of the test rig include (1) a split test section case to facilitate blade row changes at the test stand; (2) stagger adjustment capabilities for rotor blades, stators, and inlet guide vanes; (3) annular wood filler sections to provide the design flow path; and (4) a throttle vane system.

The rotor assembly is supported by a forward (roller) bearing that provides radial support and a rear (double-ball) bearing that provides both radial and axial support. A retractable support is located approximately half-way between the forward and rear bearings to support the rotor during blade-changing operations. Front bearing loads are transmitted to the outer case by means of five solid airfoil-shaped struts. A radial passage

is provided in each strut for bearing lubricant. Rear bearing loads are transmitted to the outer case by means of eight struts located aft of the throttle valve. These struts are fabricated from sheet metal and are fillet-welded into the inner and outer ducts. Eight hollow non-load-carrying struts are located aft of the exit guide vanes for instrumentation leads and the auxiliary rotor support.

Table IV-4. Blade Fatigue Life Test Results

SLOT CONFIGURATION	MODE	FREQUENCY, cps	IMPOSED STRESS LEVEL, psi	CYCLES TO FAILURE
1. No slot	1st bending	400	60,000	1.44×10^6
No slot	1st bending	394	60,000	6.4×10^6
No slot	1st bending	398	55,000	3.58×10^6
2. Long slot (10-90)* (corners rounded)	1st bending	385	25,000	5×10^6
3. Long slot (10-90) (full radius)	1st bending	385	25,000	10×10^6
4. Short slot (20-90) (full radius)	1st bending	391	35,000	3.42×10^6
Short slot (20-90) (full radius)	1st bending	408	40,000	1.72×10^6
5. Long slot (10-90) (full radius and glass bead peened)	1st bending	392	55,000	1.7×10^6
Long slot (10-90) (full radius and glass bead peened)	1st bending	390	60,000	5.2×10^6
6. No slot	1st torsion	1370	40,000	5×10^6
No slot	1st torsion	1420	48,000	0.85×10^6
No slot	1st torsion	1422	64,000	4.9×10^6
No slot	1st torsion	1400	64,000	2.5×10^6
7. Long slot (10-90) (rounded corners and glass bead peened)	1st torsion	1140	50,000	2.2×10^6
		1160	55,000	1.7×10^6
		1200	55,000	1.4×10^6
8. Slot with midspan web (10-47, 52-90) (rounded corners and glass bead peened)	1st torsion	1215	50,000	1×10^7
		1270	50,000	5.7×10^6
		1251	45,000	1×10^7

*Refers to percent span locations of slot ends.

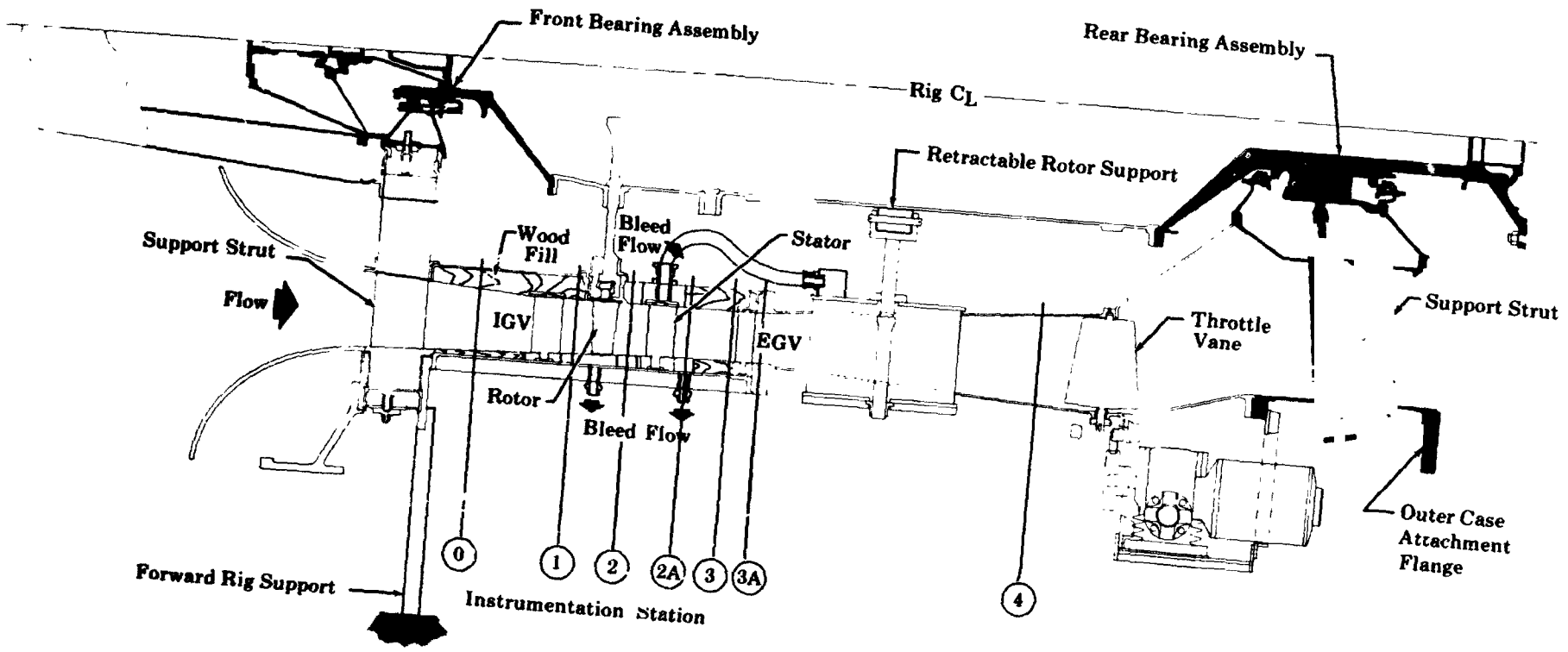

Figure IV-8. Rotating Cascade Rig

FD 14681

The rotor, supported on infinitely stiff bearings, has a calculated first critical speed of 10,300 rpm. The critical speed was calculated using a computer program, based on the Prohl method of analysis which includes the shaft variable moment of inertia, the bearing and shear flexibilities, the centrifugal stiffening of the rotor, and the shaft coupling flexibility.

C. COMPRESSOR TEST FACILITY

The compressor test facility is shown in figure IV-9. Primary components of the facility are a J75 slave engine, a two-stage exhaust ejector system, a turbine drive system, and an ASME standard inlet duct. The J75 engine supplies exhaust gases to the turbine to drive the compressor or to the exhaust ejectors for operation in a nonrotating mode. The turbine drive system is rated at 7000 maximum horsepower at 8500 rpm. The two-stage exhaust ejector system can maintain over 100 lb/sec airflow through the compressor test rig when rotating stages are not installed and the turbine drive system is disengaged.

Air enters the compressor test section through a 78-foot inlet duct, a plenum chamber, and a bellmouth inlet, and exhausts either directly to the atmosphere or through the two-stage ejector system. Airflow rate is measured in the inlet duct using a thin plate orifice. The inlet duct and plenum chamber are mounted on a track and can be rolled away from the compressor rig to facilitate test configuration and instrumentation changes.

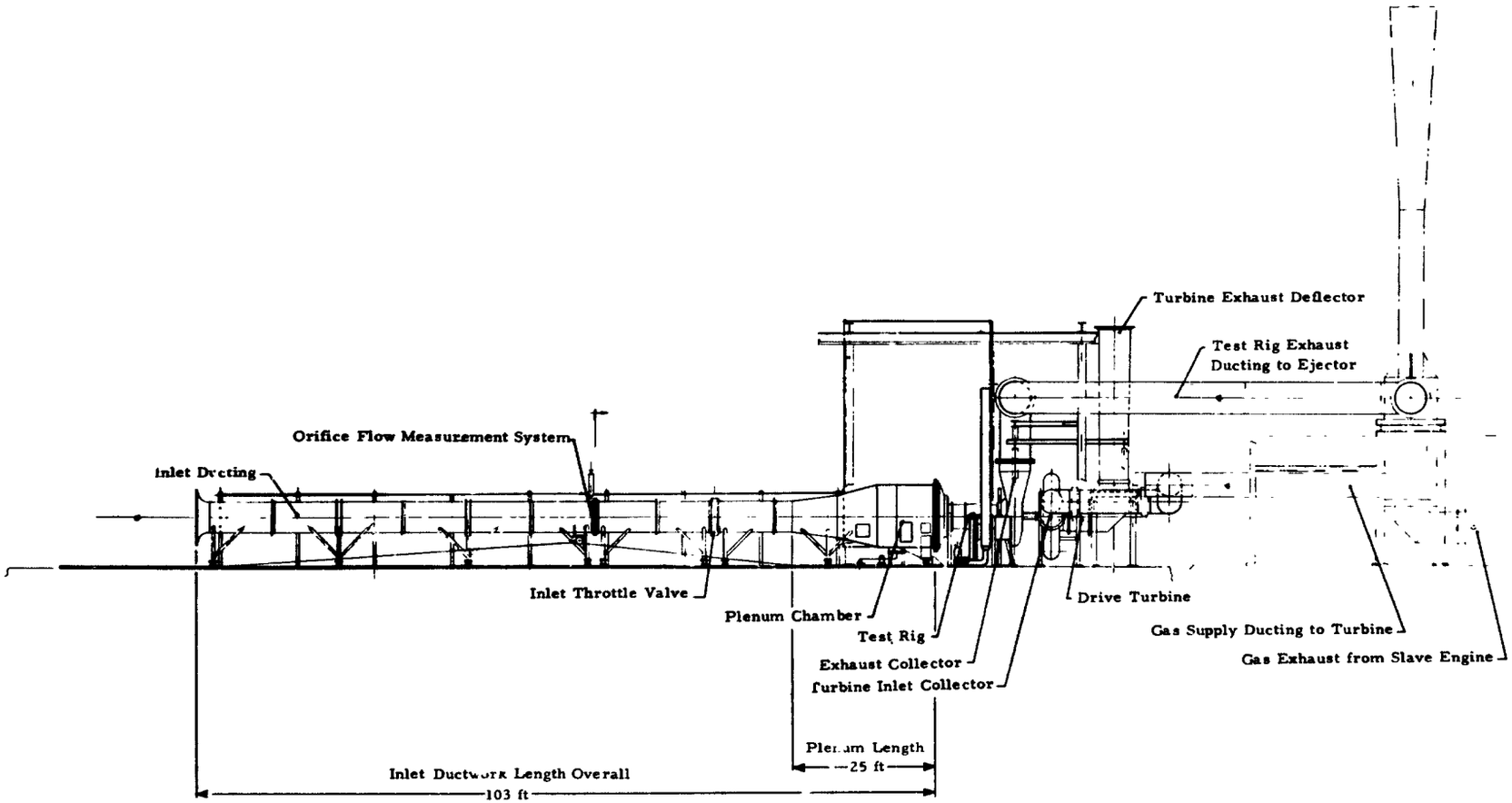

Figure IV-9. Compressor Research Facility

FD 10891A

SECTION V
SLOT FABRICATION TECHNIQUES

Three methods for machining blade slots were evaluated from the standpoint of (1) producing the desired slot configuration and (2) complexity. The evaluation of slot geometry and location resulted in slot configurations that have constant exit thickness, root to tip, and constant chord location; therefore, the main consideration for producing the desired slot geometry was that of properly accounting for blade twist.

Electrical discharge machining (EDM) is the best general method for producing the required slot geometries; three methods of EDM slot fabrication were considered in this evaluation.

The first method involves the use of a wire-cutting attachment added to the basic EDM equipment, which allows a continuous, round wire electrode to pass through the blade. A conventional EDM electrode is used to produce a hole at the slot end so that the wire can be inserted. By means of a cam arrangement on the EDM machine electrode head, the wire is moved along the slot and rotated at an angle consistent with the twist of the blade. Two wire passes produces the basic slot shape; the first pass completes one surface of the slot and the second completes the opposite side. The radii at the slot entrance and exit are blended by hard grinding to conform to radius templates. The wire cutting method produces a satisfactorily contoured blade slot, although extensive fixturing and cam arrangements are necessary. For multiple slots, four or more passes are required to produce the basic slots.

The second method involves the use of a short electrode that is traversed spanwise along the slot. This method, like the wire cutting method, would require a cam arrangement on the electrode holder to produce the desired twist as the electrode travels from one end of the slot to the other. Fixturing is required to hold the blade in a horizontal position while the airfoil is pierced prior to using the formed electrode, which is traversed with the blade in the vertical position. This method produces a satisfactory slot shape; however, like the first method, it requires considerable fixturing and cam arrangements.

The third method involves the use of a single contoured electrode, helically ground to account for blade transit along the length of the slot. This method permits cutting the desired slot geometry without rotating either blade or electrode. The blade is held in a horizontal position and tilted at a predetermined fixed angle. The contoured tool is traversed vertically into the work producing the desired shape. Figure V-1 shows the electrode shape and angle of entry for the root and tip slot positions. This technique produces exactly the desired slot geometry, with no requirement for complicated fixtures or cam arrangements. This method also eliminates the need for hand blending along the slot. A notched tool would be used to cut a double slot.

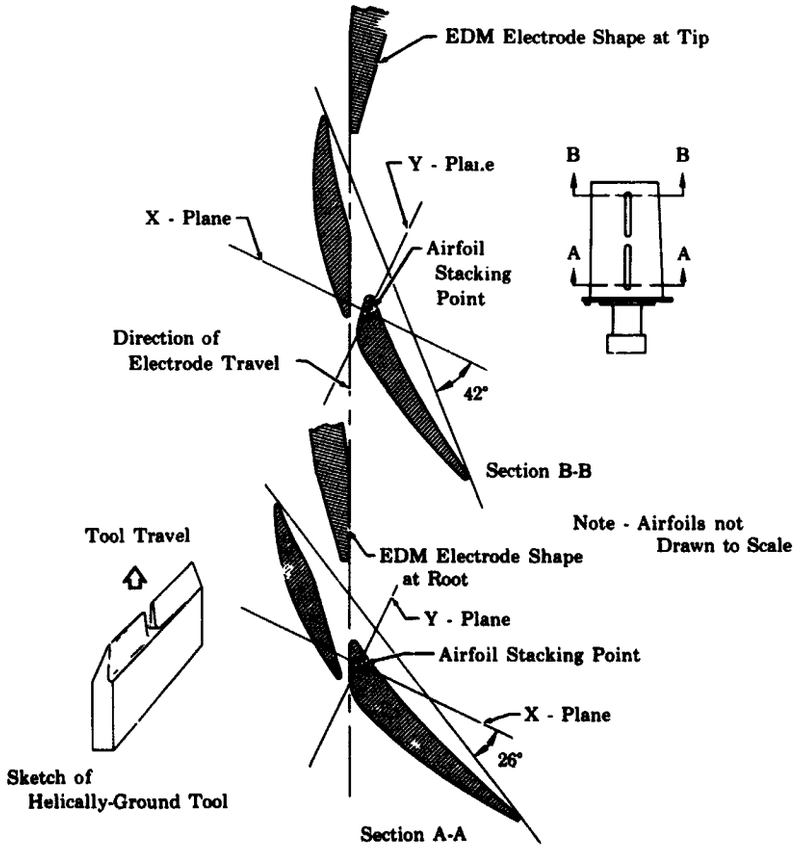

Figure V-1. Blade Slot and EDM Electrode Shape for Typical Twin Slot Airfoil FD 14734

APPENDIX A
DEFINITION OF SYMBOLS

I. VECTOR DIAGRAM NOMENCLATURE (See Figure A-1)

U	Rotor speed, ft/sec
V	Absolute velocity, ft/sec
V'	Relative velocity, ft/sec
β	Absolute air angle, deg
β'	Relative air angle, deg
$\Delta\beta$	Air turning, $\beta_1 - \beta_2$, deg

Subscripts:

1	Blade row inlet
2	Blade row exit
z	Axial component
θ	Tangential component

II. GEOMETRY DESIGN PARAMETERS (See Figure A-2)

c	Chord length, in.
o	Minimum blade passage gap, in.
o*	Critical blade passage gap, in.
S	Blade spacing, in.
t	Blade maximum thickness, in.
γ°	Blade-chord angle, deg
i_m	Incidence angle, deg
δ°	Deviation angle, deg
κ	Blade metal angle, deg
σ	Solidity, c/S
ϕ	Blade camber angle, $\kappa_1 - \kappa_2$, deg
$\bar{\omega}$	Total pressure loss coefficient, $\frac{P_1 - P_2}{P_1 - p_1}$

Note: See subscripts under paragraph I, above.

III. SLOT NOMENCLATURE (See Figure A-3)

A_2	Slot throat area $Y_2 \times \epsilon$, $in.^2$
R	Coanda radius, in.
R_p	Pressure surface radius, in.

r_1	Slot leading edge radius, in.
r_2	Slot trailing edge radius, in.
s	Spanwise dimension of slot, in.
t	Blade thickness at intersection of slot centerline and mean camber line, in.
$\dot{w}_{st}$	Total slot flow rate, lb_m/sec
$\dot{w}_p$	Primary flow rate, lb_m/sec
Y_1	Slot capture dimension, in.
Y_2	Slot throat dimension, in.
ψ	Angle formed by slot centerline and mean camber line, deg

IV. MISCELLANEOUS

A	Flow path annular area, in^2
D_F	Diffusion factor
D_L	Loading level parameter
E_{lim}	Limiting energy recovery, $1 - \left(\frac{V_s}{V_{s_{max}}}\right)^2$
ℓ	Distance from leading edge to minimum pressure point, in.
K	Flutter parameter
L	Length of pressure rise, measured from suction surface minimum pressure point, in.
M	Absolute Mach number
M'	Relative Mach number
N	Number of blades
p_p	Theoretical static pressure at intersection of slot centerline and pressure surface, for an unslotted blade, psia
p_s	Theoretical static pressure at intersection of slot centerline and suction surface, for an unslotted blade, psia
P	Total pressure, psia
q	Dynamic pressure, $\frac{1}{2}\frac{\rho}{g}V^2$, psf ($g = 32.17$ ft/sec^2)
R_ℓ	Reynolds number based on distance from leading edge to minimum pressure point
S_a	Adjustment factor - to correct for difference between predicted and observed separation points

SP	Separation point
V_s	Suction surface velocity
β_{1f}	Incidence parameter, deg
θ	Boundary layer momentum thickness, in.
ρ	Density, lb_m/ft^3
ω	Resonant frequency, cps

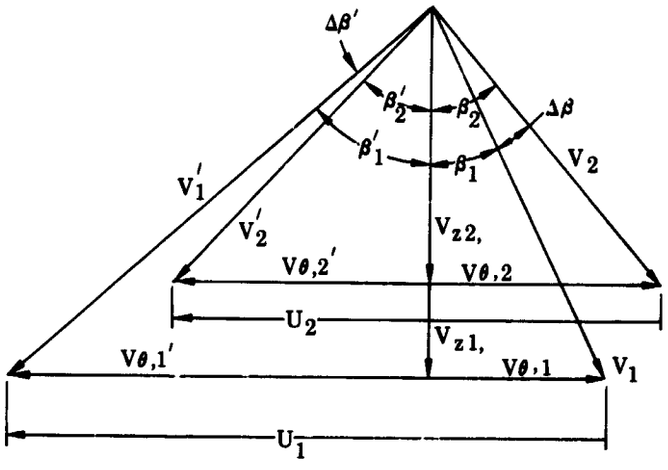

Figure A-1. Velocity Diagram Nomenclature FD 15316

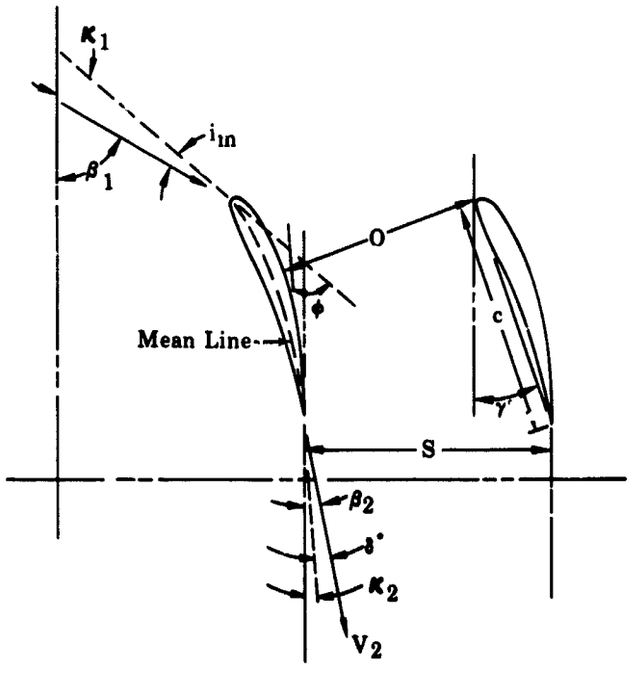

Figure A-2. Geometric Design Parameters FD 15314

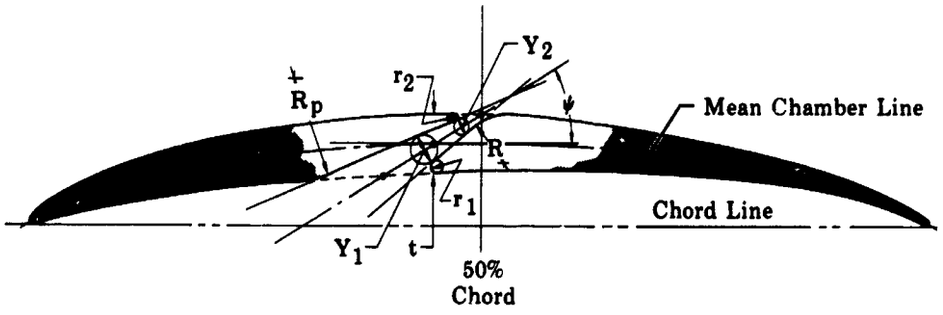

Figure A-3. Slot Geometry Nomenclature FD 15315

APPENDIX B
BLADE ELEMENT VECTOR DIAGRAM AND DESIGN DATA TABULATIONS

Data tables in this appendix are referred to in Section III. Definition of blade element vector diagram and geometry nomenclature is presented in Appendix A.

Note: Metal angles for the various airfoil series were determined as follows:

65-series - Tangent to equivalent circular arc mean lines at leading and trailing edges

63-series - Tangent to mean line at 0.5 and 95% chord locations

400-series - Tangent to mean line at leading and trailing edges.

Table B-1.
Vector Diagram Analysis Data
Inlet Guide Vane for
Flow Generation Rotor

Percent Span (from Tip)	V_1	β_1	V_2	V_{z2}	$V_{\theta 2}$	β_2	M_1	$\Delta\beta$
90	352.2	0.00	527.5	414.3	326.5	38.24	0.319	-38.24
70	352.2	0.00	518.2	404.7	323.7	38.65	0.319	-38.65
50	352.2	0.00	509.7	395.8	321.1	39.05	0.319	-39.05
30	352.2	0.00	501.8	387.6	318.7	39.43	0.319	-39.43
10	352.2	0.00	494.5	380.0	316.5	39.79	0.319	-39.79

Table B-2.
Vector Diagram Analysis Data
Flow Generation Rotor

Corrected Weight Flow 81.0 lb/sec
Corrected Rotor Speed 3850 rpm

Pressure Ratio 1.14
Efficiency, % 89

Percent Span (from Tip)	V_1'	V_{z1}	$V_{\theta 1}'$	β_1'	V_2'	V_{z2}	$V_{\theta 2}'$	β_2'	U_1	M_1'	$\Delta\beta'$	D_F
90	479.3	414.3	241.1	30.18	449.0	448.3	24.7	3.16	567.6	0.439	27.02	0.244
70	486.8	404.7	270.6	33.75	437.8	435.1	47.9	6.28	594.3	0.446	27.47	0.292
50	495.9	395.8	298.8	37.03	428.7	421.4	78.4	10.53	619.9	0.454	26.50	0.329
30	506.3	387.6	325.7	40.02	422.2	407.4	110.7	15.20	644.4	0.463	24.83	0.357
10	517.7	380.0	351.6	42.76	419.9	395.6	140.9	19.61	668.1	0.473	23.15	0.379

Table B-3.
Vector Diagram Analysis Data
Stator 1

	Percent Span (from Tip)	V_1	V_{z1}	$V_{\theta 1}$	β_1	V_2	V_{z2}	$V_{\theta 2}$	β_2	M_1	$\Delta\beta$	D_F
Unslotted	90	704.5	448.3	543.4	50.47	462.0	390.6	246.7	32.28	0.644	18.19	0.521
	70	697.3	435.1	544.9	51.38	474.4	403.9	248.7	31.61	0.636	19.77	0.506
	50	683.6	421.4	538.2	51.93	474.8	404.4	248.8	31.60	0.623	20.33	0.498
	30	667.5	407.4	528.8	52.37	470.2	399.4	248.1	31.85	0.607	20.53	0.494
	10	653.8	395.6	520.5	52.76	467.4	396.0	248.2	32.07	0.594	20.69	0.488
Slotted	90	704.5	448.3	543.4	50.47	430.7	384.0	195.1	26.93	0.644	23.53	0.596
	70	697.3	435.1	544.9	51.38	446.0	398.2	200.9	26.78	0.636	24.61	0.576
	50	683.6	421.4	538.2	51.93	448.3	400.8	200.9	26.62	0.623	25.31	0.569
	30	667.5	407.4	528.8	52.37	445.2	397.5	200.4	26.75	0.607	25.62	0.565
	10	653.8	395.6	520.5	52.76	443.7	395.8	200.6	26.88	0.594	25.88	0.560

Table B-4.
Vector Diagram Analysis Data
Stator 2

	Percent Span (from Tip)	V_1	V_{z1}	$V_{\theta 1}$	β_1	V_2	V_{z2}	$V_{\theta 2}$	β_2	M_1	$\Delta\beta$	D_F
Unslotted	90	704.5	448.3	543.4	50.47	430.3	383.3	195.6	27.02	0.644	23.45	0.596
	70	697.3	435.1	544.9	51.38	446.2	399.4	199.1	26.49	0.636	24.89	0.577
	50	683.6	421.4	538.2	51.93	448.8	401.4	200.7	26.56	0.623	25.37	0.568
	30	667.5	407.4	528.8	52.37	445.8	397.6	201.6	26.88	0.607	25.49	0.563
	10	653.8	395.6	520.5	52.76	444.3	395.3	203.0	27.18	0.594	25.58	0.556
Slotted	90	704.5	448.3	543.4	50.47	402.1	376.2	141.8	20.65	0.644	29.82	0.668
	70	697.3	435.1	544.9	51.38	420.9	394.2	147.7	20.54	0.636	30.85	0.645
	50	683.6	421.4	538.2	51.93	425.2	398.5	148.4	20.43	0.623	31.50	0.637
	30	667.5	407.4	528.8	52.37	423.6	396.5	149.0	20.60	0.607	31.77	0.633
	10	653.8	395.6	520.5	52.76	423.6	396.0	150.2	20.77	0.594	31.99	0.627

Table B-5.
Vector Diagram Analysis Data
Stator 3

	Percent Span (from Tip)	V_1	V_{z1}	$V_{\theta 1}$	β_1	V_2	V_{z2}	$V_{\theta 2}$	β_2	M_1	$\Delta\beta$	D_F
Unslotted	90	704.5	448.3	543.4	50.47	389.8	373.5	111.8	16.65	0.644	33.81	0.704
	70	697.3	435.1	544.9	51.38	410.1	393.4	115.8	16.40	0.636	34.99	0.681
	50	683.6	421.4	538.2	51.93	415.7	398.3	119.0	16.62	0.623	35.30	0.670
	30	667.5	407.4	528.8	52.37	415.2	396.8	122.1	17.10	0.607	35.27	0.665
	10	653.8	395.6	520.5	52.76	416.1	396.7	125.4	17.54	0.594	35.22	0.657
Slotted	90	704.5	448.3	543.4	50.47	371.9	36[illegible]	53.9	8.33	0.644	42.14	0.763
	70	697.3	435.1	544.9	51.38	394.1	390.0	56.9	8.30	0.636	43.08	0.741
	50	683.6	421.4	538.2	51.93	400.9	396.7	57.7	8.25	0.623	43.65	0.733
	30	667.5	407.4	528.8	52.37	401.4	396.9	59.5	8.53	0.607	43.84	0.729
	10	653.8	395.6	520.5	52.76	403.3	398.6	61.5	8.77	0.594	43.98	0.724

Table B-6.
Vector Diagram Analysis Data
Inlet Guide Vane 1

Percent Span (from Tip)	V_1	β_1	V_2	V_{z2}	$V_{\theta 2}$	β_2	M_1	$\Delta\beta$
90	426.9	0.00	519.9	479.4	201.3	22.78	0.388	-22.78
70	426.9	0.00	516.4	477.5	196.8	22.40	0.388	-22.40
50	426.9	0.00	513.2	473.3	198.4	22.74	0.388	-22.74
30	426.9	0.00	510.2	467.9	203.3	23.48	0.388	-23.48
10	426.9	0.00	507.2	462.1	209.1	24.35	0.388	-24.35

Table B-7.
Vector Diagram Analysis Data
Inlet Guide Vane 2

Percent Span (from Tip)	V_1	β_1	V_2	V_{z2}	$V_{\theta 2}$	β_2	M_1	$\Delta\beta$
90	444.6	0.00	514.0	492.6	146.7	16.58	0.405	-16.58
70	444.6	0.00	512.0	491.7	142.8	16.20	0.405	-16.20
50	444.6	0.00	510.3	489.2	145.3	16.54	0.405	-16.54
30	444.6	0.00	508.7	485.7	151.1	17.28	0.405	-17.28
10	444.6	0.00	507.0	481.8	157.9	18.15	0.405	-18.15

Table B-8.
Vector Diagram Analysis Data
Inlet Guide Vane 3

Percent Span (from Tip)	V_1	β_1	V_2	V_{z2}	$V_{\theta 2}$	β_2	M_1	$\Delta\beta$
90	403.8	0.00	436.5	436.4	5.5	0.73	0.367	-0.73
70	403.8	0.00	436.5	436.2	15.0	1.96	0.367	-1.96
50	403.8	0.00	436.4	435.8	24.0	3.15	0.367	-3.15
30	403.8	0.00	436.4	435.2	32.6	4.28	0.367	-4.28
10	403.8	0.00	436.3	434.4	40.9	5.38	0.367	-5.33

Table B-9.
Vector Diagram Analysis Data, Rotor 1

Corrected Weight Flow 95.9 lb/sec
Corrected Rotor Speed 5588 rpm

	Unslotted	Slotted
Pressure Ratio	1.31	1.37
Efficiency, %	89	91

	Percent Span (from Tip)	V_1'	V_{z1}	$V_{\theta 1}'$	β_1'	V_2'	V_{z2}	$V_{\theta 2}'$	β_2'	U_1	M_1'	$\Delta\beta'$	D_F
Unslotted	90	785.7	479.4	622.5	52.38	550.5	466.1	292.9	32.15	823.8	0.719	20.23	0.466
	70	819.3	477.5	665.8	54.33	577.5	462.9	345.3	36.72	862.6	0.750	17.61	0.458
	50	846.1	473.3	701.3	55.96	596.5	453.1	388.0	40.57	899.7	0.774	15.39	0.455
	30	868.8	467.9	732.0	57.39	611.0	440.6	423.3	43.85	935.3	0.794	13.54	0.456
	10	889.9	462.1	760.5	58.70	626.6	429.4	456.3	46.73	969.7	0.813	11.97	0.455
Slotted	90	785.7	479.4	622.5	52.38	517.5	458.4	240.3	27.66	823.8	0.719	24.72	0.535
	70	819.3	477.5	665.8	54.33	541.6	455.9	292.5	32.69	862.6	0.750	21.64	0.529
	50	846.1	473.3	701.3	55.96	558.0	443.7	338.4	37.34	899.7	0.774	18.62	0.526
	30	868.8	467.9	732.0	57.39	570.1	433.2	370.5	40.54	935.3	0.794	16.85	0.531
	10	889.9	462.1	760.5	58.70	583.4	422.3	402.6	43.63	969.7	0.813	15.07	0.532

Table B-10.
Vector Diagram Analysis Data, Rotor 2

Corrected Weight Flow 99.2 lb/sec
Corrected Rotor Speed 5366 rpm

	Unslotted	Slotted
Pressure Ratio	1.35	1.42
Efficiency, %	90	91

	Percent Span (from Tip)	V_1'	V_{z1}	$V_{\theta 1}'$	β_1'	V_2'	V_{z2}	$V_{\theta 2}'$	β_2'	U_1	M_1'	$\Delta\beta'$	D_F
Unslotted	90	811.1	492.6	644.4	52.58	533.1	472.5	246.8	27.58	791.1	0.742	25.00	0.538
	70	843.6	491.7	685.5	54.32	559.0	469.3	303.7	32.90	828.3	0.772	21.42	0.526
	50	869.3	489.2	718.6	55.73	577.1	459.1	349.7	37.29	863.9	0.795	18.43	0.520
	30	891.1	485.7	747.0	56.94	590.7	445.4	387.9	41.04	898.2	0.815	15.90	0.518
	10	911.0	481.8	773.2	58.05	606.0	431.3	425.7	44.62	931.1	0.833	13.42	0.512
Slotted	90	811.1	492.6	644.4	52.58	501.8	464.8	189.1	22.14	791.1	0.742	30.43	0.605
	70	843.6	491.7	685.5	54.32	523.9	462.5	246.1	28.02	828.3	0.772	26.30	0.596
	50	869.3	489.2	718.6	55.73	538.8	449.6	297.0	33.45	863.9	0.795	22.27	0.590
	30	891.1	485.7	747.0	56.94	549.5	437.3	332.5	37.24	898.2	0.815	19.71	0.592
	10	911.0	481.8	773.2	58.05	562.3	425.1	368.1	40.89	931.1	0.833	17.16	0.590

Table B-11.
Vector Diagram Analysis Data, Rotor 3

Corrected Weight Flow 91.4 lb/sec
Corrected Rotor Speed 4528 rpm

	Unslotted	Slotted
Pressure Ratio	1.34	1.41
Efficiency, %	90	91

	Percent Span (from Tip)	V_1'	V_{z1}	$V_{\theta 1}'$	β_1'	V_2'	V_{z2}	$V_{\theta 2}'$	β_2'	U_1	M_1'	$\Delta\beta'$	D_F
Unslotted	90	792.9	436.4	662.0	56.58	467.5	428.4	187.2	23.60	667.5	0.721	32.98	0.649
	70	811.2	436.2	684.0	57.45	479.8	417.0	237.2	29.63	698.9	0.738	27.82	0.638
	50	828.9	435.8	705.1	58.25	491.7	404.6	279.4	34.62	729.0	0.754	23.63	0.629
	30	845.8	435.2	725.3	59.01	504.9	391.7	318.6	39.11	757.9	0.769	19.90	0.619
	10	862.2	434.4	744.8	59.72	517.4	377.1	354.3	43.21	785.7	0.784	16.51	0.611
Slotted	90	792.9	436.4	662.0	56.58	439.3	422.2	121.3	16.03	667.5	0.721	40.54	0.718
	70	811.2	436.2	684.0	57.45	446.1	411.4	172.6	22.76	698.9	0.738	34.69	0.713
	50	828.9	435.8	705.1	58.25	453.8	396.9	220.0	29.00	729.0	0.754	29.25	0.706
	30	845.8	435.2	725.3	59.01	463.6	386.8	255.5	33.44	757.9	0.769	25.57	0.702
	10	862.2	434.4	744.8	59.72	473.0	374.1	289.4	37.73	785.7	0.784	21.99	0.697

Table B-12.
Geometry Design Data
Inlet Guide Vane 1

Airfoil Series: 400
No. of Blades: 50
Aspect Ratio: 1.731

Percent Span (from Tip)	κ_1	κ_2	ϕ	γ°	c	σ	t/c	δ°	$\bar{\omega}$
90	0.00	32.65	-32.65	19.42	2.262	1.072	0.060	9.87	0.138
70	0.00	32.75	-32.75	19.48	2.262	1.022	0.060	10.35	0.138
50	0.00	33.76	-33.76	20.07	2.262	0.981	0.060	11.02	0.138
30	0.00	35.68	-35.75	21.19	2.262	0.940	0.060	12.27	0.138
10	0.00	38.11	-38.11	22.60	2.262	0.903	0.060	13.76	0.138

Table B-13.
Geometry Design Data
Inlet Guide Vane 2

Airfoil Series: 400
No. of Blades 50
Aspect Ratio: 1.777

Percent Span (from Tip)	K_1	K_2	ϕ	γ°	c	σ	t/c	δ°	$\bar{\omega}$
90	0.00	24.04	-24.04	14.36	2.204	1.044	0.060	7.46	0.138
70	0.00	23.97	-23.97	14.32	2.204	0.997	0.060	7.77	0.138
50	0.00	24.84	-24.84	14.92	2.204	0.956	0.060	8.30	0.138
30	0.00	26.60	-26.60	15.87	2.204	0.916	0.060	9.32	0.138
10	0.00	28.88	-28.88	17.21	2.204	0.880	0.060	10.73	0.138

Table B-14.
Geometry Design Data
Inlet Guide Vane 3

Airfoil Series: 400
No. of Blades: 50
Aspect Ratio: 1.774

Percent Span (from Tip)	κ_1	κ_2	ϕ	γ°	c	σ	t/c	δ°	$\bar{\omega}$
90	-0.19	0.73	-0.90	0.52	2.205	1.044	0.060	0.00	0.138
70	-0.59	2.22	-2.81	1.15	2.206	0.998	0.060	0.26	0.138
50	-0.97	3.64	-4.61	1.83	2.207	0.957	0.060	0.49	0.138
30	-1.37	5.16	-6.53	2.57	2.209	0.917	0.060	0.88	0.138
10	-1.77	6.67	-8.44	3.31	2.210	0.882	0.060	1.29	0.138

Table B-15.
Geometry Design Data
Inlet Guide Vane for
Flow Generation Rotor

Airfoil Series: 63
No. of Blades: 50
Aspect Ratio: 1.530

Percent Span (from Tip)	K_1	K_2	ϕ	$\gamma°$	c	σ	t/c	$\delta°$	β
90	-26.50	42.10	-68.60	24.70	2.560	1.212	0.060	3.86	0.138
70	-26.90	42.90	-69.80	25.10	2.560	1.157	0.060	4.25	0.138
50	-27.30	43.70	-71.00	25.50	2.560	1.109	0.060	4.65	0.138
30	-27.70	44.50	-72.20	25.90	2.560	1.063	0.060	5.07	0.138
10	-28.10	45.30	-73.40	26.30	2.560	1.021	0.060	5.51	0.138

Table B-16.
Geometry Design Data
Rotor 1

Airfoil Series: 65
No. of Blades: 60
Aspect Ratio: 1.707

Percent Span (from Tip)	κ_1'	κ_2'	ϕ	$\gamma°$	i_m	0/0*	c	σ	t/c	$\delta°$	$\bar{\omega}$
90	51.69	22.44	29.25	37.11	0.69	1.230	2.210	1.250	0.075	9.71	0.058
70	53.61	28.90	24.71	41.18	0.72	1.227	2.210	1.196	0.067	7.82	0.051
50	54.98	33.84	21.14	44.35	0.98	1.242	2.210	1.149	0.059	6.73	0.050
30	55.51	38.14	17.37	46.86	1.88	1.251	2.210	1.109	0.052	5.71	0.049
10	56.12	41.99	14.13	49.08	2.58	1.259	2.210	1.071	0.044	4.74	0.046

Table B-17.
Geometry Design Data
Rotor 2

Airfoil Series: 65
No. of Blades: 60
Aspect Ratio: 1.707

Percent Span (from Tip)	κ_1'	κ_2'	ϕ	$\gamma°$	i_m	0/0*	c	σ	t/c	$\delta°$	$\bar{\omega}$
90	52.16	16.15	36.01	34.21	0.42	1.247	2.210	1.250	0.075	11.43	0.062
70	53.61	23.60	30.01	38.63	0.71	1.249	2.210	1.196	0.067	9.30	0.056
50	55.03	29.24	25.79	42.10	0.70	1.253	2.210	1.149	0.059	8.05	0.053
30	56.04	33.91	22.13	44.98	0.90	1.248	2.210	1.109	0.052	7.13	0.052
10	56.79	38.65	18.14	47.75	1.26	1.250	2.210	1.071	0.044	5.97	0.047

Table B-18.
Geometry Design Data
Rotor 3

Airfoil Series: 65
No. of Blades: 60
Aspect Ratio: 1.707

Percent Span (from Tip)	κ_1'	κ_2'	ϕ	$\gamma°$	i_m	0/0*	c	σ	t/c	$\delta°$	$\bar{\omega}$
90	58.80	6.90	51.90	32.87	-2.22	1.280	2.210	1.250	0.075	16.70	0.076
70	59.05	16.05	43.00	37.48	-1.60	1.278	2.210	1.196	0.067	13.58	0.066
50	59.45	22.96	36.49	41.25	-1.20	1.271	2.210	1.149	0.059	11.66	0.061
30	60.15	28.75	31.40	44.54	-1.14	1.261	2.210	1.109	0.052	10.36	0.056
10	61.29	34.01	27.28	47.66	-1.57	1.241	2.210	1.071	0.044	9.20	0.053

Table B-19.
Geometry Design Data
Flow Generator Rotor

Airfoil Series: 65
No. of Blades: 60
Aspect Ratio: 1.707

Percent Span (from Tip)	K_1'	K_2'	ϕ	$\gamma°$	i_m	0/0*	c	σ	t/c	$\delta°$	$\bar{\omega}$
90	31.44	-5.38	36.82	13.11	-1.26	1.449	2.210	1.250	0.075	8.54	0.051
70	35.64	-1.96	37.60	16.77	-1.89	1.459	2.210	1.196	0.067	8.24	0.046
50	39.23	2.16	37.07	20.55	-2.20	1.468	2.210	1.149	0.059	8.37	0.045
30	42.42	6.62	35.80	24.33	-2.40	1.473	2.210	1.109	0.052	8.58	0.048
10	45.36	10.87	34.49	27.85	-2.60	1.476	2.210	1.071	0.044	8.74	0.045

Table B-20.
Geometry Design Data
Stator 1

Airfoil Series: 65
No. of Blades: 58
Aspect Ratio: 1.663

Percent Span (from Tip)	K_1	K_2	ϕ	γ°	i_m	0/0*	c	σ	t/c	δ°	$\bar{\omega}$
90	52.15	22.14	30.01	37.20	-1.68	1.187	2.182	1.192	0.090	10.14	0.040
70	52.15	22.14	30.01	37.20	-0.77	1.234	2.182	1.143	0.090	9.47	0.037
50	52.15	22.14	30.01	37.20	-0.22	1.273	2.182	1.099	0.090	9.46	0.036
30	52.15	22.14	30.01	37.20	0.22	1.315	2.182	1.060	0.090	9.71	0.035
10	52.15	22.14	30.01	37.20	0.61	1.355	2.182	1.026	0.090	9.93	0.034

Table B-21.
Geometry Design Data
Stator 2

Airfoil Series: 65
No of Blades: 58
Aspect Ratio: 1.663

Percent Span (from Tip)	κ_1	κ_2	ϕ	$\gamma°$	i_m	0/0*	c	σ	t/c	$\delta°$	$\bar{\omega}$
90	53.53	14.68	38.85	34.11	-3.06	1.203	2.182	1.192	0.090	12.34	0.044
70	53.53	14.68	38.85	34.11	-2.15	1.248	2.182	1.143	0.090	11.81	0.040
50	53.53	14.68	38.85	34.11	-1.60	1.290	2.182	1.099	0.090	11.88	0.039
30	53.53	14.68	38.85	34.11	-1.16	1.333	2.182	1.060	0.090	12.20	0.037
10	53.53	14.68	38.85	34.11	-0.77	1.374	2.182	1.026	0.090	12.50	0.036

Table B-22.
Geometry Design Data
Stator 3

Airfoil Series: 65
No. of Blades: 58
Aspect Ratio: 1.663

Percent Span (from Tip)	K_1	K_2	ϕ	$\gamma°$	i_m	0/0*	c	σ	t/c	$\delta°$	$\bar{\omega}$
90	57.70	-0.64	58.34	28.52	-7.23	1.209	2.182	1.192	0.090	17.29	0.053
70	57.70	-0.64	58.34	28.52	-6.32	1.256	2.182	1.143	0.090	17.04	0.049
50	57.70	-0.64	58.34	28.52	-5.77	1.299	2.182	1.099	0.090	17.26	0.047
30	57.70	-0.64	58.34	28.52	-5.33	1.344	2.182	1.060	0.090	17.74	0.045
10	57.70	-0.64	58.34	28.52	-4.94	1.385	2.182	1.026	0.090	18.18	0.044

APPENDIX C
SUMMARY OF IBM COMPUTER PROGRAMS UTILIZED IN THE ANALYSIS AND DESIGN EFFORT

Deck No.	Description
3723	AXIAL FLOW COMPRESSOR CALCULATION - AFCC
	The AFCC program is used to perform design calculations and predict off-design performance for fan and non-fan axial flow compressors. The program uses basic aerothermodynamic equations, the continuity equation and Euler's equation of motion for compressible flow in cylindrical coordinates to predict the exit conditions for each row of an axial flow compressor. Blade losses and deviations are accounted for by correlations obtained from two-dimensional cascade test data for 400-, 65-, and circular arc airfoil series.
3893	THEORETICAL CASCADE
	The purpose of the theoretical cascade computer program is to predict the pressure coefficients on, and at selected points ahead of, an airfoil in cascade for two-dimensional incompressible flow. The method of calculation combines features of conformal mapping and source and sink singularities.
5062	CRITICAL SPEED
	This program is used to determine the critical speed of flexibly supported rotating shafts and computes the natural vibratory frequencies and vibration mode shapes.
3138	DISK STRESSES
	Tangential and radial stresses are determined for rotating disks at 1/10-inch increments with the major input of disk profile and load.

Deck No.	Description
4826	AIRFOIL STRESSES This computer program calculates blade and vane section properties at eleven radial stations and airfoil stresses due to both gas bending loads and centrifugal forces.
5036	ROTOR VIBRATION This program is used for the study of flexural vibrations for rotating disk and blade combinations. Natural frequencies of rotating disk and blade assemblies are determined together with the vibratory mode shape and relative stress distribution.
4966	BLADE VIBRATION Natural vibratory frequencies of stators and rotating blades plus relative blade stress distributions are calculated with this deck.

APPENDIX D
SLOT FLOW AREA CALCULATION

The object of this analysis was to establish a consistent method for determining the throat area for the rotor and stator slots. The procedure is based on consideration of the percentage slot flow determined in the annular cascade program and an appropriate loading level parameter, as follows:

$$\frac{\dot{w}'_{s_t}}{\dot{w}'_p} = \frac{\dot{w}_{s_t}}{\dot{w}_p} \times D_L \qquad \text{(D-1)}$$

where:

$$D_L = \frac{D_F \text{ blading}}{D_F \text{ annular cascade}}$$

where the right side of the equation is defined on the basis of annular cascade results and the prime notation refers to arbitrary blading.

The equation used to define total slot flow is:

$$\dot{w}_{s_t} = \frac{NA_2}{144}\sqrt{2g\rho(p_p - p_s)} \qquad \text{(D-2)}$$

where:

N = number of blades
A_2 = Y_2 x span (see figure III-5), $in.^2$
p_p = theoretical static pressure at intersection of slot centerline and pressure surface, psf
p_s = theoretical static pressure at intersection of slot centerline and suction surface, psf
ρ = density, lb_m/ft^3
g = gravitational constant

Writing a similar equation for an arbitrary blade slot using prime notation, and imposing the requirement of equation (D-1), the desired relationship between A_2' and A_2 can be found:

$$\frac{A_2'}{A_2} = \frac{N}{N'}\sqrt{\frac{p_p - p_s}{p_p' - p_s'}}\,\frac{\dot{w}_p'}{\dot{w}_p} \times D_L \qquad \text{(D-3)}$$

where D_L is a nondimensional loading level parameter, and has a value of 1.0 for blading that has a loading level similar to that of the annular cascade stator.

Writing A_2' and A_2 in terms of slot thickness, Y, and span, s, gives

$$\frac{Y_2'}{Y_2} = \frac{s}{s'}\,\frac{N}{N'}\sqrt{\frac{p_p - p_s}{p_p' - p_s'}}\,\frac{\dot{w}_p'}{\dot{w}_p} \times D_L \qquad \text{(D-4)}$$

Equation (D-4) was used to calculate values of Y_2'/D_L at the midspan section for the three rotor and stator configurations. The value of Y_2 corresponded to that of annular cascade configuration No. 9 (figure III-10) and $\dot{w}_p'$ corresponded to design air flow rates. The calculated values of Y_2'/D_L are listed below:

	Y_2'/D_L, in.
Rotor	
1	0.049
2	0.046
3	0.039
Stator	
1	0.048
2	0.043
3	0.036

The loading level parameter values were determined by assuming that the increase in percentage flow requirement is directly proportional to the increase in calculated midspan D-factor for the unslotted blading.* On this basis the following slot width values are obtained for an annular cascade stator D-factor of 0.528.

Rotor	Y_2'/D_L, in.	Rotor Midspan D-Factor	Y_2', in.
1	0.049	0.455	0.045
2	0.046	0.580	0.051
3	0.039	0.629	0.046
Stator		**Stator Midspan D-Factor**	
1	0.048	0.498	0.045
2	0.043	0.568	0.046
3	0.036	0.670	0.046

For convenience, a constant value of $Y_2' = 0.050$ inch was selected for the three rotor and stator configurations. This should provide a slight margin of slot flow momentum at the lower loading levels, and will ensure a minimum slot width of 0.048 inch when a tolerance of ±0.002 inch is specified.

APPENDIX E
COMPLEMENTARY VIBRATION STUDIES

Exploratory tests were conducted at the UAC Research Laboratories to determine the effects of various slot configurations on the gross vibratory characteristics of a flat plate that approximated the dynamic characteristics of the design rotor blading. The basic plate and its slotted modifications were cantilevered from the base support of the magnetic bench exciter shown in figure E-1 and driven at their natural frequencies in various resonant modes by the oscillating magnetic field of the bench exciter coils.

Figure E-1. Magnetic Bench Exciter FE 56193

The flat plates were cut from flat, cold-rolled steel stock, 2 inches wide by 1/8 inch thick, with cantilever lengths of 3.5 inches. The resonant response peak in each mode was determined both by an oscilloscope display of the dynamic response of root strain gages and by the migration of particles of carborundum grit to nodal regions during the oscillations. A camera was mounted above the test setup and photographs were taken of the nodal patterns for each mode. A composite of these photographs is shown in figure E-2. In this composite, the first column shows the reference configuration, whereas the second, third, fourth, and fifth columns show the first bending, first tension, double-torsion and second bending modes, respectively. In every case, the connection webs between slots (or between a slot and the end of a plate) comprised 10% of the plate span (or 0.35 in.), and the slots were 1/8 inch wide and located at 55% of the plate chord. Thus, the single-slotted plate was slotted over 80% of its span, the double-slotted plate over 70% of its span and the triple-slotted plate over 60% of its span.

Figure E-2 shows that the effect of slots on the first bending mode is insignificant, and the effect on the first torsion mode is measurable only for the single slot, where the frequency is reduced by approximately 10%. No data were obtained on the unslotted plate in the second bending mode, but figure E-2 shows that the differences between the one- and three-slot configurations are also insignificant.

The emergence of a double-torsion mode in the slotted configuration is not particularly surprising because, over the spanwise extent of the slot (or slots), the single plate is effectively the same as two similar plates. The existence of a relatively sharply defined mode, with nodal lines through the center of each subplate, is probably attributable to the similarity in size of each of the subplates as well as to the capability of the plates to interact through the connecting webs. A significant aspect of this mode is the large increase in frequency associated with an increase in the percentage of span occupied by the web. Even with the single-slotted plate, the frequency of the double-torsion mode (3860 cps) is greater than 3 times the frequency of the first torsion mode (1156 cps). Thus, although the effective chord of each subplate of the slotted configuration has been halved, the frequency

has been tripled; the resulting product of blade semichord and torsional frequency, $c\omega$, of the single-slotted plate is considerably greater than that of the unslotted plate. The multislotted plates have even greater increases in the value of $c\omega$.

Consider now the possibility of torsional stall flutter in the double-torsion mode. As previously stated, the reduction in the blade semichord will be more than compensated for by the increase in frequency, the $c\omega$ of one of the subplates in the single-slotted configuration will be approximately 1.5 times the $c\omega$ of the basic first torsion mode. Therefore, if there is sufficient flutter margin for the first torsion mode, there will be an even greater margin for the single-slotted double-torsion mode.

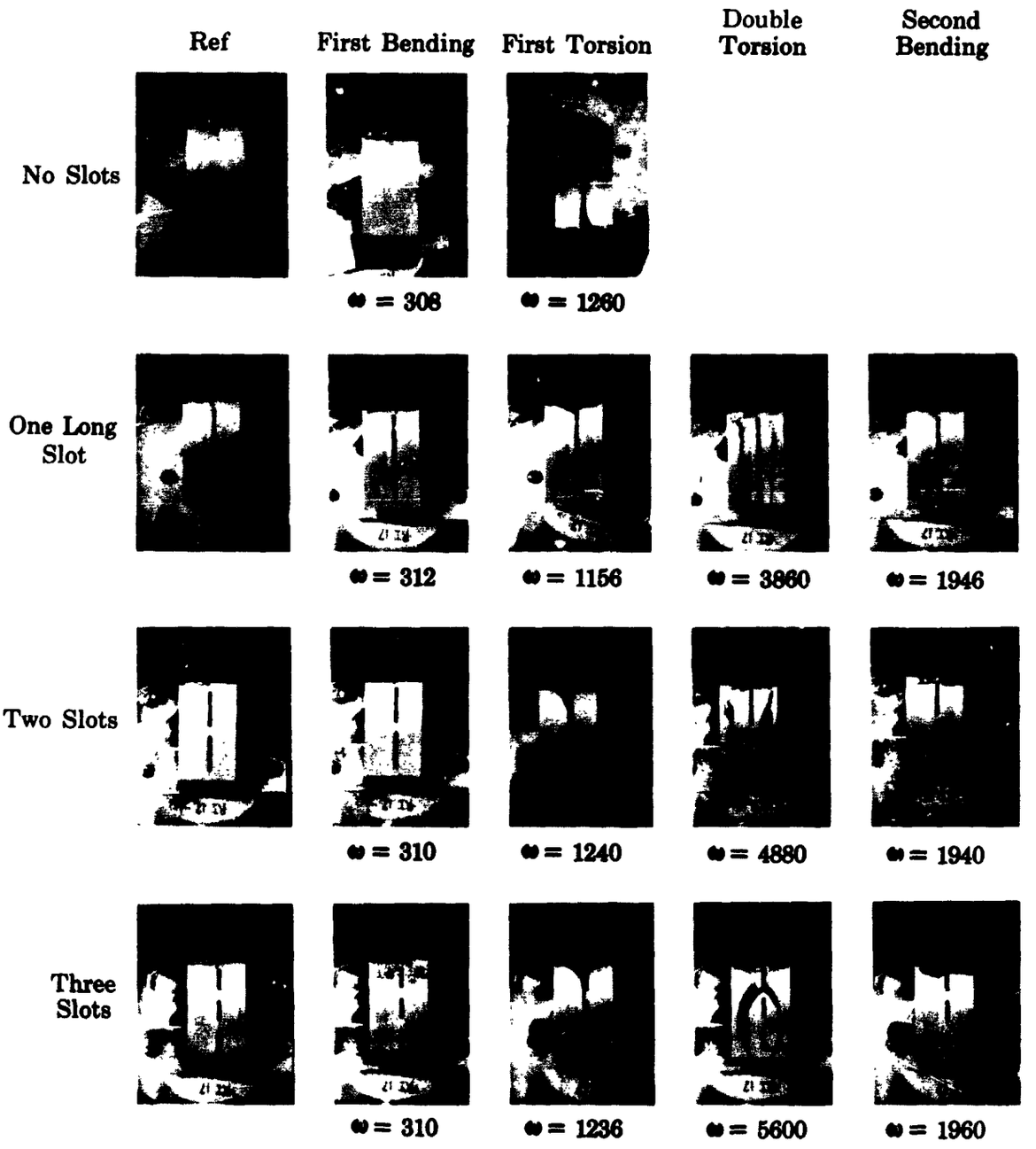

Figure E-2. Vibration Nodal Patterns FD 14684